UNIVERSITY OF HELSINKI

https://helda.helsinki.fi

Both plume and arc : origin of Neoarchaean crust as recorded in Veligallu greenstone belt, Dharwar craton, India

Dey, Sukanta; Pal, Sayantan; Balakrishnan, S.; Halla, Jaana; Kurhila, Matti ...

2018-09

Elsevier B.V.

http://hdl.handle.net/10138/314629

Dey, S, Pal, S, Balakrishnan, S, Halla, J, Kurhila, M & Heilimo, E 2018, 'Both plume and arc : origin of Neoarchaean crust as recorded in Veligallu greenstone belt, Dharwar craton, India', Precambrian Research, vol. 314, pp. 41-61. https://doi.org/10.1016/j.precamres.2018.04.019

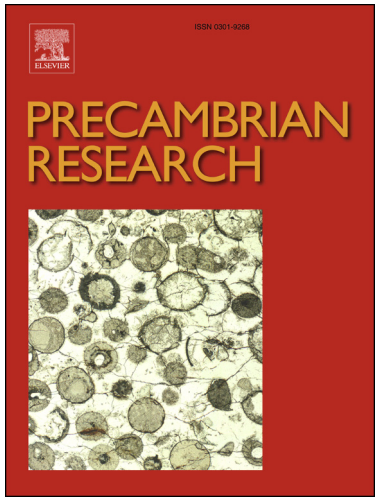
Downloaded from Helda, University of Helsinki institutional repository. https://helda.helsinki.fi

This is an electronic reprint of the original article.

This reprint may differ from the original in pagination and typographic detail.

Please cite the original version.

Accepted Manuscript



Both plume and arc: origin of Neoarchaean crust as recorded in Veligallu greenstone belt, Dharwar craton, India

Sukanta Dey, Sayantan Pal, S. Balakrishnan, Jaana Halla, Matti Kurhila, Esa Heilimo

PII: S0301-9268(17)30450-3
DOI: https://doi.org/10.1016/j.precamres.2018.04.019
Reference: PRECAM 5069

To appear in: *Precambrian Research*

Received Date: 2 August 2017
Revised Date: 16 April 2018
Accepted Date: 18 April 2018

Please cite this article as: S. Dey, S. Pal, S. Balakrishnan, J. Halla, M. Kurhila, E. Heilimo, Both plume and arc: origin of Neoarchaean crust as recorded in Veligallu greenstone belt, Dharwar craton, India, *Precambrian Research* (2018), doi: https://doi.org/10.1016/j.precamres.2018.04.019

This is a PDF file of an unedited manuscript that has been accepted for publication. As a service to our customers we are providing this early version of the manuscript. The manuscript will undergo copyediting, typesetting, and review of the resulting proof before it is published in its final form. Please note that during the production process errors may be discovered which could affect the content, and all legal disclaimers that apply to the journal pertain.

ACCEPTED MANUSCRIPT

Re-Revised Manuscript without showing track changes

Both plume and arc: origin of Neoarchaean crust as recorded in Veligallu greenstone belt, Dharwar craton, India

Sukanta Dey[a]*, Sayantan Pal[a], S. Balakrishnan[b], Jaana Halla[c], Matti Kurhila[d,e], Esa Heilimo[f]

[a] *Department of Applied Geology, Indian Institute of Technology (Indian School of Mines), Dhanbad 826 004, India*
[b] *Department of Geology, Pondicherry University, Pondicherry 605 014, India*
[c] *Finnish Museum of Natural History, FI 00014 University of Helsinki, Finland*
[d] *Geological Survey of Finland, Mintec, Tutkijankatu 1, FI-83500 Outokumpu, Finland*
[e] *Geological Survey of Finland, P.O. Box 96, FI-02151 Espoo, Finland*
[f] *Geological Survey of Finland, P.O. Box 1237, FI-70211 Kuopio, Finland*

* Corresponding author (e-mail: geodeys@gmail.com;
Ph: +91-326-2235450; Fax: +91-326-2296616)

ABSTRACT

Several profound changes, including those involving formation of the continental crust, occurred on Earth during the Neoarchaean Era. However, the tectonic settings associated with Neoarchaean crustal growth are not well understood and vigorously debated. The Neoarchaean Veligallu greenstone belt, eastern Dharwar craton hosts a variety of ultramafic, mafic and felsic volcanic rocks. Whole-rock elemental and Nd isotope data along with zircon U-Pb dating on these rocks provide significant insights into the origin and tectonic setting of Neoarchaean crust formation. The volcanism in the Veligallu belt started with ~2.67 Ga tholeiitic basalts derived from shallow melting of a slightly depleted mantle (ε_{Ndt} = +0.6 to +1.1). Moderate negative Nb anomalies, slightly elevated Th/Yb and LREE, and an absence of evidence for crustal contamination are consistent with extraction of these basalts from a mantle source weakly metasomatized by subducted slab-derived fluids in an incipient oceanic arc setting. As the arc matured, clastic sediments started forming with concurrent emplacement of komatiites, komatiitic basalts and ferropicrites showing strong signatures of contamination with continental crust (negative Nb and Ti anomalies, LREE enrichment and negative ε_{Ndt}). In the final stage (~2.58 Ga), a variety of felsic volcanic rocks (sodic trachyandesite, high Mg# andesite, rhyolite, calc-alkaline andesite) formed. The rock association and distinct geochemical signatures (enrichment of LILE, negative Nb and Ti anomalies, Mesoarchaean Nd model ages and inherited older zircons) suggest a continental

ACCEPTED MANUSCRIPT

margin arc environment which contained older crust. The evolutionary history of the Veligallu belt implies that both the arc- and plume-related processes, and their interplay contributed significantly to the growth of Neoarchaean crust.

Keywords:

Neoarchaean; Veligallu greenstone belt; Dharwar craton; Volcanic rocks; Geochemistry; Crustal evolution

1. Introduction

Several profound changes occurred on Earth between 2.7 Ga and 2.6 Ga, such as, a major pulse in igneous activity, enhanced mantle depletion, a peak in the production of juvenile continental crust and widespread formation of orogenic gold and massive-sulphide deposits (Barley et al., 1998; Condie, 1998; Reddy and Evans, 2009). These events are commonly attributed to the 2.7 Ga worldwide mantle plume activity which was followed by increased rate of subduction, development of accretionary orogens, collision between continental blocks, crustal reworking and, possibly, formation of the first supercontinent Kenorland (Condie, 1998, 2004; Barley et al., 2005). Late Neoarchaean (2.7–2.5 Ga) greenstone belts act as windows into these profound changes. However, the nature of tectonics and actual mechanism(s) of growth of continental crust during the Neoarchaean Era remain contentious (Condie and Benn, 2006; Bedard, 2006 and 2013; Wyman, 2013). Many authors argue that Neoarchaean geodynamic processes were similar to those of the Phanerozoic including plume–subduction/lithosphere interaction, subduction accretion, thrusting and imbrication, strike–slip faulting, continental rifting and orogenic collapse (Pease et al. 2008; Wyman and Kerrich, 2009; Polat et al. 2009). Others suggested non-plate tectonic models which assume production of TTG (tonalite-trondhjemite-granodiorite) by melting of basaltic protocrust followed by mostly gravity-driven processes like sinking of dense greenstone belt mafic-ultramafic rocks and diapiric rising of TTG batholiths (Hamilton, 2011). Repetitive delamination of dense restitic lower crust causing refertilization of rising mantle plumes and formation of new melts is one widely cited variant of the non-plate tectonic model (Bedard et al., 2013).

The eastern Dharwar craton (EDC) is a collage of several greenstone belts interleaved with 2.7–2.5 Ga granitoid bodies (Fig. 1). Available limited geochronological data suggests that the main period of EDC mafic-ultramafic volcanism was coeval with the global ~2.7 Ga

ACCEPTED MANUSCRIPT

peak in juvenile crust generation (Balakrishnan et al., 1990; Naqvi et al., 2002; Anand and Balakrishnan, 2010; Jayananda et al., 2013a; Khanna et al., 2016). A felsic volcanic event is also recorded at 2.59–2.55 Ga (Sarma et al., 2008; Jayananda et al., 2013a; Dey et al., 2015). Previous on EDC volcanic rocks mostly concentrated on whole-rock elemental data (e.g. Naqvi et al., 2006; Manikyamba et al., 2008; 2009; Manikyamba and Kerrich, 2011; Khanna et al., 2015). Correlation of globally recognized Neoarchean events with those of the EDC is difficult because of insufficient geochronological (e.g. U-Pb zircon) and isotope geochemical data (e.g. Nd isotope). Also, the extent of mantle depletion and mantle heterogeneity below the EDC are still not adequately constrained (Dey, 2013).

The Veligallu greenstone belt in the EDC (Fig. 1) hosts a variety of igneous rocks (De Smeth et al., 1985; Ramam and Murty, 1997; GSI, 2006; Subba Rao and Sesha Sai, 2012; Khanna et al., 2015, 2016) and can provide significant insights into the mechanism(s) of Neoarchaean crustal growth and geodynamic setting. In this contribution we present petrographic and geochemical (whole-rock elemental) information coupled with Nd-isotope and U-Pb zircon data on metavolcanic rocks of the Veligallu greenstone belt to constrain their source and petrogenesis. The nature juvenile crust formed, extent of crustal reworking and possible tectonic setting are discussed which may have wider implications in understanding Neoarchaean crustal evolution.

2. Geology of the Dharwar craton

The Archaean Dharwar craton is divided into two blocks with different crust formation histories (Chadwick et al., 2000; Jayananda et al., 2006; Chardon et al., 2008). The western block (western Dharwar craton or WDC) consists of 3.35–3.30 Ga polyphase granitoids (mainly TTG) along with 3.4–3.0 Ga highly deformed, amphibolite to granulite facies supracrustal rocks of the Sargur schist belts (Swami Nath and Ramakrishnan, 1981; Meen et al., 1992; Peucat et al., 1993; Jayananda et al., 2008, 2015; Maya et al., 2016). Younger volcano-sedimentary basins, preserved in the 2.9–2.55 Ga Dharwar-type greenstone belts, unconformably overlie these granitoids and Sargur rocks (Chadwick et al., 1992; Kumar et al., 1996). The last phase of plutonism in the WDC is represented by minor 2.6 Ga potassic granites (Jayananda et al., 2006).

ACCEPTED MANUSCRIPT

In the eastern block (eastern Dharwar craton or EDC) only vestiges of 3.3–3.0 Ga granitoids are preserved (Jayananda et al., 2000; Bidyananda et al., 2011). Otherwise, granitoids include 2.72–2.53 Ga syntectonic (with respect to the formation of regional penetrative fabric) TTGs and transitional TTGs, 2.56–2.51 Ga late tectonic sanukitoids, the atypical 'Closepet-type' granitoid and anatectic potassic granitoids, and Palaeoproterozoic post-tectonic A-type granitoids and syenites (Jayananda et al., 1995, 2000, 2018; Dey et al., 2003, 2009, 2012, 2014, 2016; Moyen et al., 2003; Ram Mohan et al., 2013). The granitoid bodies are interspersed with narrow greenstone belts (Kolar-type; Fig. 1), the latter containing greenschist to amphibolite facies volcanic rocks of diverse compositions including high-Mg andesites, boninites, Nb-enriched basalts, adakites, rhyolites, komatiites and tholeiitic, alkaline and high-Mg basalts (e.g. Balakrishnan et al., 1990; Naqvi et al. 2006; Manikyamba et al., 2008, 2009, 2015, 2017; Rogers et al., 2007; Manikyamba and Kerrich, 2011, 2012; Dey et al., 2015; Jayananda et al., 2013a; Khanna et al., 2015). Metasedimentary rocks such as iron formations, cherts, greywackes and metapelites occur in association with metavolcanic rocks.

The whole Dharwar craton shows N–S to NNW trending structural fabric, which is attributed to Neoarchaean (2.56–2.51 Ga) transcurrent shear deformation due to shortening (Chardon et al., 2008). Zircon U-Pb and monazite chemical dating indicated that the Dharwar craton was affected by thermal events at 3.2–3.0, 2.62 and 2.55–2.51 Ga (Jayananda et al., 2012, 2013b; Peucat et al., 2013).

The Neoarchaean tectonic setting of the EDC is controversial. Suggested models include

(i) *Active margin model:* Successive accretion of arcs or pieces of against an older foreland (the WDC) in a convergent setting resulting in oblique convergence which partitioned into subduction parallel NNW-SSE sinistral transpression and subduction perpendicular NE-SW shortening (Chadwick et al., 2000, 2003, 2007). The greenstone belts of the EDC formed in intra-arc basins, whereas the Dharwar-type greenstone belts of the WDC represent back-arc basins. Convergence resulted in accretion of diverse plume- and arc-related terranes (Krogstad et al., 1995; Balakrishnan et al., 1999; Manikyamba and Kerrich, 2012).

ACCEPTED MANUSCRIPT

(ii) *Mantle plume model:* A mantle plume supplied heat softening a pre-existing crust (Chardon et al., 1998, 2002; Jayananda *et al.* 2000). This induced inverse diapirism, metamorphism, partial melting of crust and granitic magmatism.

(iii) *Combined arc-plume model:* Plume-related, juvenile 2.7–2.65 Ga mafic-ultramafic and felsic magmatism followed by emplacement of arc-related 2.58–2.52 Ga felsic volcanic and TTG and calc-alkaline plutonic rocks. Subsequent mantle plume activity at 2.52 Ga caused crustal reworking, granulite facies metamorphism and final cratonization of the EDC (Moyen et al., 2003; Jayananda et al., 2013a; Peucat et al., 2013). Some authors suggested that between 2.56-2.51 Ga the EDC was a hot orogen with soft, buoyant crust formed by magmatic accretion in a convergent set up. The convergence resulted in lateral constrictional flow of EDC lower crust against the older and rigid WDC (Chardon et al., 2008, 2011; Chardon and Jayananda, 2008).

3. Geology of the Veligallu greenstone belt

The Veligallu greenstone belt is exposed over a N-S trending narrow tract in the south-eastern part of the EDC (Fig. 2). In the southern part of the belt, mafic volcanic rocks and banded iron formations (BIF) are the major rock types. The mafic rocks are massive to well-foliated, fine to medium grained and, at places, pillowed (Fig. 3a). They consist mainly of hornblende, plagioclase and actinolite-tremolite with accessory opaque minerals (± biotite) (Fig. 3b). Subparallel alignment of prismatic and/or fibrous grains of actinolite-tremolite and hornblende defines the foliation. In some samples hornblende occurs also as porphyroblasts. Often hornblende grains are being replaced by actinolite-tremolite. Sericitization and saussuritization of plagioclase and chloritization of the hornblende and biotite grains are the common alteration types. These rocks contain subvertical NNW-SSE trending bodies of gabbro probably representing subvolcanic intrusions. The gabbros consist mainly of sericitized plagioclase laths and prismatic igneous clinopyroxene grains with subordinate opaque and orthopyroxene grains. The clinopyroxene grains show replacement by actinolite-tremolite and chlorite along grain boundary. Some of the gabbroic bodies contain very coarse dark euhedral to subhedral hornblende grains (Fig. 3c). The interstitial spaces are occupied by anhedral plagioclase grains (Fig. 3d). Some of the samples of this rock have preserved intergranular texture (Fig. 3e).

ACCEPTED MANUSCRIPT

The northern part of the Veligallu greenstone belt is, however, dominated by quartz-muscovite schists (psammopelites) with subordinate tuffs, BIF, agglomerates and cherts. Felsic and mafic-ultramafic volcanic/sub-volcanic rocks occur as subvertical conformable layers and lenses intercalated with the quartz-muscovite schist (Fig. 3f). Commonly, the mafic-ultramafic layers are a few meters thick and 10s of meters long. Only a few are wider (20–40 m), extending up to 10 km in length. The ultramafic units consist mainly of tremolite-actinolite with subordinate anthophyllite, opaque and relict hornblende grains (Fig. 3g). Alteration products include serpentine and talc. The mafic bodies are fine to coarse grained consisting of flaky, prismatic to fibrous actinolite-tremolite, prismatic to wedge-shaped hornblende and clouded plagioclase laths with minor opaque grains. In some samples stubby to subrounded actinolite-tremolite grains form porphyroblasts. Often the hornblende grains are replaced by actinolite-tremolite. Chloritic and biotitic alterations are noted in some samples. Generally subparallel alignment of actinolite-tremolite and hornblende grains impart a weak to strong foliation within the mafic-ultramafic rocks.

Layers of felsic volcanic rocks are common within the Veligallu greenstone belt. The most prominent one extends along the eastern margin of the belt for about 25 km (Fig. 2). These rocks are weak to strongly foliated, commonly banded (Fig. 3h), and medium-grained rocks. They consist mainly of quartz, plagioclase and hornblende (± biotite ± chlorite) with accessory opaque, zircon and apatite grains (Fig. 3i). Some of the rocks are plagioclase-porphyritic. Hornblende grains are commonly altered to actinolite-tremolite. The foliation is generally defined by parallel alignment of hornblende, biotite and chlorite grains (Fig. 3j).

Rocks of the Veligallu greenstone belt were affected by greenschist to amphibolite facies metamorphism and strong deformation, obscuring the stratigraphic relationship among the lithounits. Three generations of deformations were recorded in the greenstone belt (Ramam and Murty, 1997; GSI, 2006; Subba Rao and Sesha Sai, 2012). The first is represented by mesoscopic tight to isoclinal folds (F_1) having steep to vertical plunging axes. The major N-S trending foliation within the greenstone belt is axial planar to F_1. The F_2 folds with gentle SSW plunge are regional in nature. These folds have NNW-SSE trending axial trace. Broad warps with subvertical ENE-WSW trending axial planes represent the third generation folds (F_3). Shear zones/faults trending N-S, NW-SE and NE-SW cut across the volcano-sedimentary package of the belt.

ACCEPTED MANUSCRIPT

The Veligallu greenstone belt is associated with a variety of granitoids. Unpublished zircon U-Pb age data of the authors show that the oldest among them is a 2.66 Ga banded TTG gneiss. These gneisses, at places, form basement for the quartz-muscovite schist. Other granitoids include 2.56–2.53 Ga porphyritic granodiorites, anatectic biotite granites and two-mica granites. Intrusion of these younger granitoids possibly dismembered the greenstone belt in to two N-S trending arms (Fig. 2).

4. Geochemistry

Details of whole-rock major and trace element determination, whole-rock Sm-Nd isotope analysis and secondary ion mass spectrometry (SIMS) single grain zircon U–Pb dating are reported in the Appendix 1.

4.1 Major and trace elements

The major and trace elemental compositions of the Veligallu metaigneous rocks are presented in Table 1. The southern mafic rocks (SiO_2 = 47.7–54.7 wt%) are classified mostly as tholeiitic basalts using the criteria of Ross and Bedard (2009) (Figs. 4a, b). These rocks (henceforth called southern basalts) display moderate to high MgO, TiO_2 and $Fe_2O_3^t$, moderate to low Al_2O_3, and low Cr, Ni and Mg number (0.63–0.35) (Table 1, Fig. 5). REE patterns are flat with 7 to 28 times enrichment of absolute REE contents compared to the chondritic values (Fig. 6a). The primitive mantle (PM) normalized plots also show flat patterns except for moderate negative Nb anomaly and minor negative Ti and Y anomalies (Fig. 6b). From Zr to Lu (fluid immobile elements) the pattern is parallel to that of normal mid-ocean ridge basalt (N-MORB), although the absolute concentrations are generally lower than those of N-MORB. Unlike MORB, the fluid-mobile elements (Th and La to Nd) are not depleted. On the Nb/Yb vs. Th/Yb diagram the basalts mostly plot slightly above the mid-ocean ridge basalt–ocean island basalt (MORB-OIB) array (Fig. 7).

The northern mafic-ultramafic rocks, barring the sample VB273, show high contents of MgO (34–9.5 wt%), Ni (1759–216 ppm) and Cr (3630–763 ppm). Three of these samples are classified as komatiites, three as komatiitic basalts and two as basalts on the Al_2O_3-(Fe_2O_3+TiO_2)-MgO triangular plot of (Jenson, 1976) (not shown). The absolute TiO_2, REE, Zr and Y and abundances show wide variations which increase with decreasing MgO content

ACCEPTED MANUSCRIPT

(Fig. 5). Besides, Cr and Ni display good positive correlation with MgO. The rocks have variable chondrite-normalized enrichment of LREE and flat HREE patterns (Fig. 6c). PM-normalized patterns display varying degree of enrichment of highly incompatible elements (Th and LREE) with distinct negative Nb and Ti anomalies (Fig. 6d). Samples with higher LREE contents also display negative Zr and Hf anomalies. The Al_2O_3/TiO_2 ratios scatter widely (38 to 5 against a chondritic value of 20) (Fig. 8). Three samples (VB273, VB288 and VB294) have distinctly higher Fe_2O_3, CaO, HFSE (Ti, Zr and Nb), Y and V contents with correspondingly higher Ti/Y, Ti/Zr, Ti/Gd, and lower Mg# and Al_2O_3/TiO_2 ratios compared to other northern mafic-ultramafic samples (Table 1). All of the northern mafic-ultramafic rocks mostly plot significantly above the MORB-OIB array in the Nb/Yb vs. Th/Yb diagram (Fig. 7).

The felsic volcanic rocks display a wide range of elemental compositions with low to high MgO (0.6 to 6 wt%) and Mg# (0.26–0.58). They vary from andesite, trachyandesite, dacite to rhyolite in compositions in the SiO_2 vs. Zr/TiO_2 plot of Winchster and Floyd (1977) (not shown). The chondrite normalized REE patterns show variable LREE enrichment, whereas HREE patterns range from flat to depleted (Fig. 6e). These samples show PM-normalized enrichment of Th and LREE with distinct negative Nb and Ti anomalies (Fig. 6f). The HREE- and Y-depleted silicic sample VAV208 shows high values for Na_2O, Sr (649 ppm), Na_2O/K_2O (~2) and Sr/Y (130), and low total ferromagnesian element contents. These features indicate adakitic affinity (Martin et al. 2005).

4.2 Zircon U-Pb dating

SIMS zircon U-Pb data for sample VAV127 are presented in Table 2. The sample was collected 4 km S65°E of Veligallu (Fig. 2). It is a medium-grained sub-volcanic rock of trachyandesite composition consisting dominantly of quartz and plagioclase with interstitial chloritized biotite and prismatic hornblende grains (Fig. 3i). Sub parallel alignment of biotite grains has imparted a moderate foliation within the rock. The zircon grains in the sample are prismatic with clear oscillatory zoning suggesting their igneous origin (Fig. 9a). Seventeen analyses on seventeen grains yielded moderate U (112–577 ppm) and low to moderate Th (61–410 ppm) with Th/U values ranging from 0.29 to 0.82. The analyses are concordant to variably discordant (Fig. 9b). Three concordant points yield a combined concordia age of 2579±4 Ma (MSWD = 3.7). Seven among the nine most concordant analyses (discordance

ACCEPTED MANUSCRIPT

<5%) define a similar weighted mean $^{207}Pb/^{206}Pb$ age of 2584±5 Ma (MSWD = 2.1). This age is interpreted as the age of crystallization of the rock. Two other sub-concordant analyses (#5 and 13) provide an older mean $^{207}Pb/^{206}Pb$ age of 2605±5 Ma (MSWD = 0.14) and probably represent inherited zircons. In addition, four analyses (#8, 10, 12 and 14) are distinctly older whose $^{206}Pb/^{207}Pb$ ages range from 2919 to 2651 Ma. These ages are minimum estimates, as the analyses are discordant. These older zircons are also inherited.

4.3 Nd isotope

Nd isotope data are presented in Table 3. Eleven samples of the southern tholeiitic basalts define an errochron age of the 2673 ± 200 Ma (MSWD = 2.3), with an initial $^{143}Nd/^{144}Nd$ value of 0.50921±0.00026 and a corresponding initial ε_{Nd} value of +0.7 (Fig. 10). Absence of correlation between ε_{Nd} and 1/Nd indicates that the collinear array is not due to mixing between basaltic material and continental crust. In spite of the large error, the age is consistent with the whole-rock Sm-Nd ages reported from the initial phase of mafic magmatism in other Neoarchaean greenstone belts of the eastern Dharwar craton, which cluster around 2.7 Ga (Balakrishnan et al., 1990; Naqvi et al., 2002; Anand and Balakrishnan, 2010). Khanna et al. (2016) obtained a similar whole-rock Lu-Hf age estimation (2640 ± 150 Ma; MSWD = 28) for the basaltic rocks of the Veligallu belt.

In the northern part of the Veligallu belt mafic-ultramafic bodies are concordantly intercalated with the quartz-sericite schists. At some places these supracrustal rocks occur unconformably over the ca. 2.66 Ga gneissic TTG granitoids (GSI, 2006) constraining the upper age limit of the former. The ca. 2.58 Ga felsic volcanic layer occurring along the eastern margin of the Veligallu belt is considered, on the basis of stratigraphic relation, to be the youngest igneous rock of the belt (Ramam and Murty, 1997; GSI, 2006). Considering these facts, the time of formation of the northern mafic-ultramafic rocks are conservatively taken as 2.66−2.6 Ga. Six analysed samples of the northern mafic-ultramafic rocks show mostly negative initial ε_{Nd} (Table 3).

Samples VAV127, VAV60 and VAV3 were collected over a small area from the same felsic volcanic layer running along the eastern margin of the Veligallu belt (Fig. 2). Among them, VAV127 yielded a U-Pb zircon age of 2.58 Ga. We surmise that these lithologies represent ca 2.58 Ga age due to field relationships (spatial closeness and

ACCEPTED MANUSCRIPT

stratigraphic equivalence). The first two samples (trachyandesite and rhyolite respectively) are characterized by negative initial ε_{Nd} values (−3.7 and −2.8 respectively) with old Nd T_{DM} ages (3.24 and 3.14 Ga respectively) (Table 3 and Fig. 10b). Sample VAV3, however, shows a juvenile character with a positive initial ε_{Nd} value (+1.3).

Jayananda et al. (2013) reported a SHRIMP zircon U-Pb age of 2697±5 Ma for a adakitic felsic volcanic rock from the Veligallu greenstone belt constraining the age of adakitic magmatism in the belt. This age is also similar to the southern tholeiitic basalt. The sample VAV208 also have adakitic composition and shows a positive initial ε_{Nd} value (+2.5) at 2.7 Ga. The Nd T_{DM} age (2.83 Ga) is close to its presumed crystallization age.

5. Assessment of alteration

Only fresh-looking samples were collected in the field, which were further screened for alterations (e.g. silicification and carbonatization) during microscopic study. Rocks of the Archaean greenstone belts generally were affected by sea-floor weathering, hydrothermal alteration and metamorphism. Commonly Al, Ti, Mg, REE (La–Lu), HFSE (Th, Nb, Ta, Zr and Hf), Y, Ni, Sc, V, Cr and Co are considered less likely to be mobile in such situations (Alt, 1999; Polat and Hofmann, 2003; Masters and Argue, 2005). These elements are mainly used for petrogenetic interpretation in this work. In the case of the felsic rocks and the southern tholeiitic basalts, most of these elements show coherent trends in chondrite normalized REE patterns and primordial mantle normalized spider diagrams attesting to the validity of this assumption (Fig. 6). They also have low LOI values (0.3–2.5 wt%) (Table 1). However, the northern komatiites and komatiitic basalts have higher LOI (mostly 2.1–5.7 wt%) signifying fluid activity. They display slightly jagged patterns in the spidergrams along with negative Eu anomaly suggesting that some of the REE could have been mobilized. Yet these rocks consistently display enrichment of LREE, flat HREE and negative Nb and Ti anomalies. In addition, good correlations exist between MgO and oxides/elements like Al_2O_3, TiO_2, Zr, Hf, Y, Yb, V and Ni (Fig. 5). These elements also display coherent magmatic trends with respect to Zr (not shown) which is generally considered to be immobile. These facts indicate that the data of the northern komatiites and komatiitic basalts can be used for petrogenetic interpretations with proper caution.

ACCEPTED MANUSCRIPT

6. Petrogenesis

6.1 Southern tholeiitic basalts

6.1.1 Mantle source characteristics

Fluids, especially those in subduction zones, can carry LILE (Th and LREE) and metasomatize parts of the adjacent mantle (Pearce and Peate, 1995). In contrast, the HFSE (Nb, Ti, Zr, Hf) and HREE (Gd to Lu) are more or less immobile except in the case of transport by melts (Pearce, 2008). Therefore, the HFSE/Yb ratios and HFSE ratios provide information on the nature of the pre-metasomatized mantle source of basaltic magmas (Pearce, 1996, 2008; Pearce and Peate, 1995; Condie, 2003, 2005). The southern basalts are confined within the MORB-OIB array in the Zr/Yb vs Nb/Yb (Fig. 11a) plot (after Pearce and Peate, 1995) suggesting absence of any external input of these elements into the source mantle. However, the moderate shifting of the samples towards the E-MORB reflects a less depleted mantle source compared to that of the NMORB. In the Zr/Y and Nb/Y diagram also (Condie, 2005) these basalts plot near primitive mantle extending towards the enriched mantle component (Fig. 11b). The Ti/Nb and Zr/Nb ratios (Table 1) are generally higher than the chondritic ratios (1800 and 16 respectively) and, but lower than those of the NMORB (2765 and 32 respectively) (McDonough and Sun, 1995; Arevalo and McDonough, 2010). Therefore, these elemental ratios suggest that the southern basalts were derived from a depleted mantle source, although the extent of depletion was to some extent less than that of a typical NMORB mantle source. Nevertheless, it is expected that the mantle source would be less depleted than the modern day NMORB source. So, it could still be the normal Archaean NMORB source.

6.1.2 The crustal signature

The positive initial ε_{Nd} values of the southern basalts (+0.3 to +1.1 at 2.67 Ga; Table 3) also suggest a mantle source with small degree of LREE depletion. However, except two samples showing minor chondrite-normalized LREE depletion (La/Sm_{cn} = 0.8 and 0.9), others have flat to slightly enriched LREE patterns (La/Sm_{cn}= 1.02 to 1.6) (Fig. 6a). Further, the southern basalts generally plot slightly above the MORB-OIB mantle array in the Nb/Yb vs. Th/Yb plot (Fig. 7). These facts indicate introduction of minor amount of LREE and Th, the 'crustal signature', into the mantle source. This crustal signature, as also represented by

ACCEPTED MANUSCRIPT

negative Nb and Ti anomalies in the PM-normalized plot (Fig. 6b), may be acquired by fluid-fluxing of mantle carrying LREE and Th in preference to HFSE (e.g. Nb) (Pearce, 2008). Alternatively, contamination with continental crust during ascent of the basalt may impart this geochemical signature. However, the magnitudes of the crustal signatures are less in the southern basalts compared to what would be expected in the case of interaction with continental crust. For example, crustally contaminated Archaean basalts display $(La/Sm)_{PM}$ >1.5, Th/Ce >0.05 and Nb/Th <5 (Kerrich et al. 1999; Condie, 2003). In contrast, the southern basalts predominantly have lower values for the first two ratios, whereas Nb/Th ratios are mostly higher reflecting absence of crustal contamination. The initial ε_{Nd} values also do not show any relationship with the magnitude of PM-normalized Nb and Ti anomalies or $(La/Sm)_{PM}$ values.

Except for garnet fractionation, the Zr/Y ratio does not significantly change by fractionation of olivine, pyroxene and plagioclase. On the other hand continental crust has considerably higher Zr/Y value and might introduce obvious change in Zr/Y ratios in to basalts ascending through it. Involvement of garnet can be ruled out in case of southern basalts on the basis of flat HREE patterns. These basalts display flat pattern in the Y vs. Zr/Y plot without any distinct change in Zr/Y ratios (Fig. 12). Crustal contamination therefore seems to be unlikely for the southern basalts considering all the geochemical features. In conclusion, these basalts were possibly produced by partial melting of a fluid-fluxed, slightly depleted mantle source at shallow depth.

6.1.3 Source melting and factional crystallization

Primary melts in equilibrium with mantle generally have high Mg# (>70) and Cr (500–600 ppm) and Ni contents (250–350 ppm) (Perfit et al., 1980). The southern basalts display relatively lower Mg# (0.35–0.63), Cr (<20 to 330 ppm) and Ni (30-280) values indicating that they do not represent primary magma and the parental magma have undergone some fractional crystallization. The decrease in Ni with MgO suggests olivine fractionation (Fig. 5). Cr depletes very fast with increase of Y (not shown) pointing to fractionation of Cr-spinel. The Zr/Y ratio remains constant with increasing Zr or Y (Fig. 12). This fact also points towards fractional crystallization of olivine. The TiO_2 and V contents increase along with decrease of MgO contents. This probably reflects that Fe-Ti rich minerals (e.g. titanomagnetite) were not the fractionating phases. The flat HREE pattern indicate absence of

ACCEPTED MANUSCRIPT

garnet either as residual or fractionating phase, consistent with shallow melting of a spinel-lherzholite mantle.

6.2 Northern komatiites, komatiitic basalts and basalts

6.2.1 Source characteristic and melt generation

The northern mafic-ultramafic rocks occur as intercalated concordant bodies within the metasediments. Cross cutting relationships were not observed during the course of this study, and the detailed mapping and drilling carried out by the Geological Survey of India (Subba Rao et al., 2012). This is consistent with a volcanic or near-volcanic origin of the northern mafic-ultramafic rocks. These rocks display a wide range of compositions. The three samples with the highest MgO contents (26–34 wt%) are characterized by near-chondritic Al_2O_3/TiO_2 (~23) and flat HREE patterns similar to 'Munro-type' komatiites or Al-undepleted komatiites (Arndt et al., 2008). This type of komatiites are common within ~2.7 Ga greenstone belts globally. Experimental works and geochemical modelling indicated that 'Munro-type' komatiites formed in mantle plumes at shallow depths and pressures at about 5–7 GPa (Arndt, 1984; Herzberg, 1999; Arndt et al., 2008).

The relation between komatiites and associated high-MgO basalts is a controversial issue. Suggested mechanisms of formation of komatiitic basalts include fractionation and/or crustal contamination of komatiite magma, partial melting of a heterogeneous mantle source and variable partial melting within a homogeneous source mantle (Arndt et al., 2008). The northern komatiites and komatiitic basalts show some collinearity in the Harker diagrams (Fig. 5). However, the relation between them is complex given the fact that three of the northern basalt samples (VB273, VB294 and VB288) have relatively higher Fe_2O_3(T), CaO, HFSE (Ti, Zr and Nb), V, Y and HREE contents, and Nb/Y ratios coupled with lower Al_2O_3/TiO_2 (5.4–12.4) (Figs. 5, 8 and 11) making them similar to ferropicrites identified from several greenstone belts of the Superior craton (Stone et al., 1995; Goldstein and Francis, 2008). Komatiitic basalts with elevated Fe, LREE, Ti and Nb contents and lower Al_2O_3/TiO_2 ratios (~6) have been reported from the ~2.7 Ga Boston Creek Flow, Abitibi greenstone belt, Superior craton (Stone et al., 1995). Melting of a depleted mantle source, mixed with a highly enriched small-degree melt fraction at mantle depth, was suggested for generation of these rocks (Stone et al., 1995). However, the low Al_2O_3/TiO_2 ratios of the Boston Creek samples

ACCEPTED MANUSCRIPT

are mainly due to their distinctly low Al_3O_3 contents. Also, unlike the Veligallu samples, they have fractionated HREE patterns and positive Nb anomalies. Instead, the Veligallu samples bear more similarity with the Fe- and Ti-rich ~2.1 Ga picrites of northern Finland, where the low Al_2O_3/TiO_2 ratios are mainly the result of higher abundances of TiO_2 rather than low Al_2O_3 contents (Hanski, 2001). The distinctive chemical characteristics of these ferropicrites suggest that they cannot be derived from the same mantle source as that of the komatiites and komatiitic basalts. Geochemical modelling coupled with Nd isotope data and phase relation studies indicated that alteration, crustal contamination and fractional crystallization cannot explain the formation of the Archaean ferropicrites (Barnes and Often, 1990; Goldstein and Francis, 2008). Rather, low-pressure (<5 GPa) melting of discrete Fe- and incompatible element-rich domains within mantle can explain the origin of these ferropicrites (Hanski, 2001; Goldstein and Francis, 2008; Milidragovic et al., 2014; Milidragovic and Francis, 2016).

Another alternative possibility is that the komatiites and komatiitic basalts represent cumulates of the southern tholeiitic basalts (Khanna et al., 2016). However, these two suites of rocks are spatially separated: the tholeiitic basalts are restricted to the southern part of the Veligallu belt, whereas the komatiites and komatiitic basalts occur intercalated with the quartz-sericite schists in the northern part (Fig. 2). Further, these two suites do not plot on the same trends in the Harker diagrams (Fig. 5). They display distinct REE and multielemental patterns (Fig. 6), trace element ratios (Figs. 4,7,11 and 12) and Nd isotope signatures (Fig. 13). These facts preclude the suggested cumulate relationship between the komatiites-komatiitic basalts and tholeiitic basalts.

6.2.2 Crustal contamination

Archaean komatiitic magmas had very high temperatures (Sobolev et al., 2016) and, therefore, high capability to assimilate crustal rocks (Sparks, 1986). Crustal contamination have been proposed to explain LREE-enriched komatiites and associated basalts with negative Nb anomaly from a number of Archaean terrains (e.g. Perring et al., 1996; Puchtel et al., 1997). The relatively higher SiO_2 contents (at the level of MgO), LREE enriched character, distinct negative Nb anomalies and mostly negative initial ε_{Nd} values of the northern mafic-ultramafic rocks indeed point towards significant interaction with continental crust. Further, in the Th/Yb vs. Nb/Yb diagram these rocks plot much above the MORB-OIB

ACCEPTED MANUSCRIPT

mantle array (Fig. 7). In the Y vs. Zr/Y plot they show distinct increase in Zr/Y with Y extending towards the upper continental crust (Fig. 12). The transitional character (between tholeiitic and calc-alkaline nature; Fig. 4b) is also consistent with contamination by continental crust.

In detail, the process of crustal contamination may, however, vary from thermal erosion of the underlying crustal material (Perring et al., 1996) to assimilation and fractional crystallization during the ascent through the crust (Mungall, 2007). The northern mafic-ultramafic rocks are intercalated with metamorphosed siliciclastic sediments and subordinate felsic volcanic rocks. A scenario of intermittent volcanic flows coeval with the deposition of sediments would apply for them. In such cases, crustal assimilation can take place by thermal erosion of the underlying silicic metasediments. On the $^{147}Sm/^{144}Nd$ vs. ε_{Nd} plot the northern mafic-ultramafic rocks, except the sample VB301, plot on trends consistent with contamination with the Veligallu metasediments or granitic gneisses of the eastern Dharwar craton (Fig. 13). The sample VB301 seems to be more fractionated one with distinctly higher absolute LREE and Th contents.

Notably, the most LREE enriched samples among the northern mafic rocks show distinct primordial mantle-normalized depletion of Zr and Hf with respect to LREE, which is generally considered as signature of crustal contamination (e.g. Milidragovic et al., 2014). The Veligallu metasedimentary rocks display similar LREE enrichments and distinct negative Nb and Ti anomalies. However, they have rather PM-normalized Zr and Hf enrichment. Even the TTG gneisses, forming the basement for the Veligallu metasediments, the Veligallu intermediate to felsic volcanic rocks and the average upper continental crust show slight to moderate positive Zr-Hf anomaly. The average lower continental crust displays only slight negative Zr and Hf anomaly. Possibly, emplacement of the high-temperature mantle-derived parental magma of the northern mafic-ultramafic rocks was responsible for formation of low-degree crustal melts (highly enriched in LREE) with retention of zircon in the residue (Hoffmann et al., 2016). Assimilation of this crustal melts and attendant fractional crystallization can explain the negative Zr and Hf anomalies of the most LREE-enriched samples of northern mafic rocks. In conclusion, the northern part of the Veligallu greenstone belt hosts mantle plume-derived Munro-type komatiites, komatiitic basalts and ferropicrites, which were emplaced onto and extensively contaminated by continental crust.

ACCEPTED MANUSCRIPT

6.3 Felsic rocks – diverse origin

The felsic volcanic rocks of the Veligallu belt display diverse compositions. They show somewhat scattered distribution for many elements (e.g. Al, La, Zr, Y, Yb and V) (Fig. 5). Geochemical proxies for crustal contamination or slab melt (e.g. Th/Nb, La/Sm, La/Nb) do not display any trend with SiO_2, MgO or Zr (not shown). In the Zr/Y vs. Y and εNd vs. $^{147}Sm/^{144}Nd$ diagrams too, the felsic volcanic rocks do not show any trend (Figs. 12 and 13). Therefore, the observed variation within the felsic volcanic rocks cannot be explained by crustal contamination or mantle metasomatism by slab melt. They were most likely to have originated through distinct petrogenetic pathways.

The 2.58 Ga highly sodic trachyandesite sample VAV127 is characterized by higher Al_2O_3, HFSE (Zr, Nb, Hf, Th and U), REE and Ga contents compared to the other Veligallu felsic volcanic rocks (Table 1). This is a common Archaean rock type that has a contentious origin (e.g. Said et al., 2012 vs. Barnes and Van Kranendonk, 2014). The enriched and fractionated LREE pattern, negative Eu anomaly and flat HREE pattern coupled with PM-normalized depletion of Nb and Ti and distinctly negative $\varepsilon_{Nd2.58Ga}$ value (−3.7) testify involvement of a crustal material with either plagioclase as a fractionating phase or a residual phase after source melting. However, the intermediate level of SiO_2 (59 wt%) and undepleted V, Cr and Ni contents (183, 130 and 70 ppm respectively) indicate that melting of mafic to felsic crustal lithologies followed by fractionation cannot explain the composition of the sample. It is difficult to constrain the origin of such magma from a single sample. A possible mechanism could be fractional crystallization of a metasomatized mantle-derived alkaline mafic magma and simultaneous assimilation of a crustal rock or mixing with melts derived from sialic crust (Hoffmann et al., 2016) with significantly old isotopic signature. The nearby quartz-muscovite schist, characterized by elevated Al_2O_3 and incompatible trace element contents and highly negative $\varepsilon_{Nd2.58Ga}$ (Figs. 6d and 13), is a possible assimilate. The high Na_2O content and low K_2O and Rb contents are notable. However, given the singular nature of the sample and the high mobility of these elements, it is not possible to pinpoint the origin of these features.

The sample VAV3 is a calc-alkaline andesite with high Mg# (0.58), Cr (270 ppm) and Ni (310 ppm). The positive initial ε_{Nd} value (+1.3) suggest a depleted mantle source, although the magnitude of this depletion is lower than that of the contemporary depleted mantle

ACCEPTED MANUSCRIPT

($\varepsilon_{Nd2.6Ga}$ ~4). The chondrite normalized moderately enriched LREE pattern and PM normalized negative Nb and Ti anomalies indicate contribution from crust (Fig. 6). Therefore, it is suggested that this sample represents a high Mg# andesite derived from a depleted mantle source. Either the source mantle was modified by crustal contaminant or the mantle-derived magma interacted with continental crust.

The sample VAV60 is a rhyolite enriched in LREE and Th (16 ppm). The negative Eu anomaly and flat HREE pattern, negative Nb and Ti anomaly (Fig. 6) and negative initial Nd value (−2.8) suggest a low pressure origin and involvement of continental crust with older history. However, the high Mg# (0.48), Ba, Cr and Ni (1118, 120, and 60 ppm respectively) along with low contents of Al_2O_3, Rb (73 ppm) and Ga suggest contribution from mantle. An origin by partial melting or fractional crystallization of a mantle-derived high Mg# andesite (similar to VAV3) followed by contamination/assimilation with crustal material is consistent with the geochemical features of the rock (Kelemen et al., 2014).

The silicic nature of the sample VAV208 along with high Na_2O and Sr, and low total ferromagnesian element contents (Fe_2O_3+MgO+MnO+TiO_2 = 4.9 wt%) and K_2O/Na_2O ratio (0.5) suggest it to be similar to high-silica adakites (Martin et al., 2005). The low Y and Yb contents and corresponding high Sr/Y ratio (130) and fractionated HREE pattern indicate high-pressure origin with garnet either as residual or fractionating phase (Martin et al. 2005; Richards and Kerrich, 2007; Moyen, 2010; Castillo, 2012). Jayananda et al. (2013) reported a zircon U-Pb age of 2697±5 Ma Ga for a Veligallu volcanic rock of very similar geochemistry constraining the age of adakitic magmatism within the belt. The ε_{Nd} value of the sample VAV208 at 2.7 Ga (+2.5) and negative Nb and Ti anomalies imply a juvenile source (metabasalt) with arc signature. The low MgO content and Mg# value preclude a direct contribution from mantle.

The sample VAV220 is a calc-alkaline andesite characterized by depleted HREE (Yb = 1.2 ppm, La/Yb = 18) and moderately high Sr/Y ratio (26) suggesting high-pressure origin involving garnet in their petrogenesis. The sample have moderate Mg# (0.44), Cr (200 ppm) and Ni (80 ppm) which are lower than those of the mantle-derived andesite sample VAV3. Moreover, VAV220 has distinctly higher LREE and Th contents indicating fractionation and/or contamination with more felsic crust. It also shows prominent primordial mantle-normalized negative Nb and Ti anomalies reflecting an arc or crustal contamination signature.

ACCEPTED MANUSCRIPT

7. Discussion

7.1. Mantle heterogeneity below the eastern Dharwar craton

Isotope (especially Nd, Hf and Os) and elemental compositions of mantle-derived rocks from many cratons indicate significant heterogeneity within the Archaean mantle (e.g. Jahn et al., 1980; Vrevsky et al., 1996; Hoffmann and Wilson, 2017). A significant number of Neoarchaean (~2.7 Ga) basalt samples from the Kolar greenstone belt of the EDC show initial ε_{Nd} values >3 suggesting existence of considerably depleted mantle (Balakrishnan et al., 1990; Dey, 2013). Mantle-derived ~2.7 Ga metabasalts from the Ramagiri and Hutti greenstone belts indicate moderately depleted sources (initial ε_{Nd} = +1.4 to +3.5; Zachariah et al., 1997; Anand and Balakrishnan, 2010). The southern basalts of the Veligallu belt reflect a slightly depleted mantle source (initial ε_{Nd} = +0.3 to +1.1). Trace elemental and isotopic signatures do not indicate significant crustal contamination for none of these EDC basalts (Balakrishnan et al., 1990; Anand and Balakrishnan, 2010; Dey, 2013). The wide range of Nd isotope compositions therefore implies either significant regional chemical heterogeneity or introduction of material derived from older continental crust lowering the Sm/Nd ratio of parts of the mantle at about 2.7 Ga.

The occurrence of ferropicrites in the Veligallu greenstone belt, along with those reported earlier from the Kolar greenstone belt (Rajamani et al., 1985, 1989), also documents significant compositional heterogeneity in the form of Fe-rich domains within the Neoarchaean mantle beneath the EDC. It is becoming increasingly apparent that ferropicrites are volumetrically minor but common components of Neoarchaean greenstone belts of many cratons like Superior, Slave, Yilgarn, Kaapvaal and Karelia (Stone et al., 1995; Francis et al., 1999; Goldstein and Francis, 2008; Milidagrovic et al., 2014; Milidragovic and Francis, 2016). The Mg/(Mg+Fe) ratios (Mg#) of such Fe-rich mantle domains were probably low (0.76–0.84)) compared to those of the more abundant pyrolytic mantle (Mg# = 0.88–0.92) (Milidragovic et al., 2014; Milidragovic and Francis, 2016).

7.2. Evidence of older (Mesoarchaean to Palaeoarchaean) crust

ACCEPTED MANUSCRIPT

Earlier studies reporting Nd (± Pb ± Sr ± Hf) isotope compositions of greenstone belt mafic-ultramafic volcanic rocks and granitoids proposed that EDC is made up mostly of Neoarchaean juvenile crust (Balakrishnan et al., 1990; Peucat et al., 1993; Krogstad et al., 1995; Jayananda et al. 2000; Khanna et al., 2016). However, distribution of depleted mantle Nd model ages suggests that Palaeoarchaean to Mesoarchaean crust is abundant in the western part of the EDC extending from the Chitradurga shear zone to the Kolar greenstone belt (Fig. 1) (Dey, 2013; Dey et al., 2016). This zone is considered as a transitional domain ('Central Dharwar province') representing the eastern margin of the older (>3.0 Ga) WDC remobilized and reworked during 2.58–2.51 Ga hot orogenic magmatism (Jayananda et al. 2013a; Peucat et al., 2013). Sparse data exist on the Neoarchaean (2.7–2.5 Ga) crust preserved to the eastern part of the EDC (east of the Kolar greenstone belt), which is claimed to be juvenile (Jayananda et al. 2013a; Peucat et al., 2013). However, ≥ 3.0 Ga inherited zircons were recorded from the Neoarchaean felsic volcanic rocks of the Kolar, Kadiri and Hutti greenstone belts from the eastern part of the EDC (Jayananda et al., 2013a). Some of these felsic volcanic rocks and associated granitoids yielded Palaeoarchaean to Mesoarchean (3.6–2.9 Ga) Nd depleted mantle model ages (Jayananda et al., 2013a; Dey et al., 2014, 2015; Rajamanickam et al., 2014).

Further evidence of older crust comes from the felsic volcanic rocks of the Veligallu greenstone belt, exposed in the far east of the EDC, displaying Mesoarchaean (3.2–3.0 Ga) Nd depleted mantle model ages (Table 3) and inherited zircon (sample VAV127). Notably, the northern Veligallu komatiites, ferropicrites and komatiitic basalts preserve Nd isotope signature that reveal interaction with Mesoarchaean crust. Cryptic Palaeoarchaean to Mesoarchaean isotope signatures in dominantly Neoarchaean terrains are common in other cratons too (e.g. Yilgarn, Karelia and Superior; Champion and Sheraton 1997; Mikkola et al. 2011; Wyman et al. 2011). Accretion of microcontinental plates with older crustal history can explain these isotope signatures (Schmitz et al., 2006; Dey et al., 2016). Most of this older crust in the EDC was lost either by erosion (forming clastic sediments within the greenstone belts) or reworking during the 2.58–2.51 Ga hot orogenic magmatism (Chardon et al. 2011; Manikyamba and Kerrich 2012; Dey 2013; Dey et al., 2014, 2015).

7.3. Tectonic setting

7.3.1. Southern basalts – juvenile magmatism in a possible incipient oceanic arc

ACCEPTED MANUSCRIPT

The southern basalts do not display evidences for contamination by continental crust. Therefore, the higher La/Yb and Th/Yb ratios compared to mantle array and negative PM-normalized Nb and Ti anomalies (Figs. 6 and 7), may be acquired though metasomatism of the source mantle before partial melting. Introduction of fluid-mobile trace elements, LREE and Th in preference to HFSE and HREE in to an oceanic sub-arc mantle wedge through slab-derived fluids can impart these geochemical signatures (Pearce and Peate, 1995). Rudnick (1995) suggested that basalts derived from subduction-modified mantle have La/Nb (>1.4). Most of the southern basalts have marginally higher La/Nb ratios (mostly range 1.1–1.9) indicating derivation from a mantle-wedge source slightly modified by slab-derive fluid. Slab dehydration generally produces basalts with lower Th enrichment (Th/Ce <0.1) compared to those characterized by melting of slab sediments (Hawkesworth et al, 1994). All the southern basalts samples are characterized by low Th/Ce (0.02–0.06) indicating slab dehydration only. The subduction contribution increases with maturity of the arc. Basalts generated in incipient arcs or protoarcs are generally tholeiitic and carry a small subduction component (lower Th/Nb) compared to mature arcs (Ishizuka et al., 2011; Wang et al., 2015). The southern basalts represent a similar case and, therefore, an incipient oceanic arc seems to be a likely tectonic setting for their generation. The adakite sample VAV208 was probably also formed through young oceanic slab melting during this initial period of oceanic arc formation (Castillo, 2012). However, it is noted with caution that rocks with adakite signature can form in a variety of tectonic settings (Bedard, 2006).

7.3.2. Komatiites, ferropicrites and komatiitic basalts – mantle plume ascent in a continental margin or arc environment

These rocks display prominent elemental and isotopic signatures of contamination by continental crust. They are associated with abundant quartzose clastic metasediments and felsic tuffs. The metasedimentary rocks have siliceous compositions (SiO_2 ~ 66 wt%) with fractionated LREE and distinct PM-normalized negative Nb and Ti anomalies (unpublished data of the authors; Fig. 6). A majority of them show negative Eu anomaly with relative flat HREE patterns indicative of derivation from an evolved granitic source. We suggest mantle plume ascent into a volcanically active continental margin environment (e.g. Puchtel et al., 1997; Mole et al., 2014). The related komatiites, ferropicrites and komatiitic basalts were

ACCEPTED MANUSCRIPT

emplaced simultaneously with the deposition of continent-derived clastic sediments and felsic tuffs.

Khanna et al. (2016) reported whole-rock Hf isotope data on five samples of the Veligallu ultramafic rocks whose $\varepsilon Hf_{2.7Ga}$ varies between +3.2 to +5.6. This is in contrast to the mostly negative εNd(t) values of the Veligallu ultramafic and associated mafic rocks (komatiites, ferropicrites and komatiitic basalts) reported in this study (Table 3). The decoupling of Hf from Nd, and the presence of ferropicrites could be related to incorporation of garnet pyroxenites in the depleted mantle sources, possibly during delamination (Hoffmann and Wilson 2017). This is compatible with a scenario proposed by Bédard (2006), where komatiites and ferropicrites form in response to delamination. The garnet pyroxenites may be the restites of TTG formation and, being denser than the mantle, can delaminate. At the present moment, it is very difficult to test the decoupling model because the Sm-Nd and Lu-Hf data were collected from different samples. However, we note that delamination can occur in an arc setting (Tatsumi, 2000; Lee and Anderson, 2015). Komatiites and komatiitic basalts are considered to be high-temperature rocks. Their emplacement within sedimentary rocks like quartz-muscovite schists (psammopelites) is expected to result in contamination. So our data and model of crustal contamination is more consistent with the geological setting.

7.3.3. Felsic volcanic rocks – addition of juvenile crust and crustal reworking in a mature arc

By 2.58 Ga, felsic volcanism became common in the area. The sub-arc mantle became progressively more metasomatized by fluids derived from melting of slab basalt and/or sediment. Partial melting of this metasomatized, previously depleted mantle probably generated LREE-enriched high Mg# andesite (VAV3) with juvenile character ($\varepsilon_{Nd2.58Ga}$ = +1.3) (Grove et al., 2003; Kelemen et al., 2014). This juvenile magma possibly underwent variable fractionation and assimilated continental crust producing rocks ranging in composition from andesites to rhyolites. The Na-, LILE- and HFSE-rich trachyandesite sample (VAV127) represent minor alkaline magmatism within the arc. Similar alkaline, incompatible trace element-rich trachyandesites, contemporaneous with calc-alkaline volcanic rocks, have been reported from recent subduction zones (e.g. Nelson and Livieres, 1986; Parat et al., 2005) as well as Archaean greenstone belt associations (Said et al., 2012;

ACCEPTED MANUSCRIPT

Szilas et al., 2012, 2016; Barnes and Van Kranendonk, 2014). They are interpreted to form during the final stage of volcanic arc evolution.

The rock association (high Mg# andesites, andesites, rhyolites and trachyandesites), evidence of widespread explosive volcanism (agglomerates and tuffs) and distinct geochemical signatures (enrichment of LILE and negative Nb and Ti anomalies) suggest an arc setting for these felsic volcanic rocks. The Mesoarchaean depleted mantle Nd model ages (Table 3) coupled with presence of inherited older zircons (2.92–2.65 Ga, $^{207}Pb/^{206}Pb$ ages) (Fig. 9) indicate reworking or assimilation of older continental crust. A continental margin arc environment, where crustal reworking generally is a major process (DeCelles et al., 2009), is the likely tectonic setting for emplacement of these volcanic rocks.

7.4. Implications for the mechanism(s) of Neoarchaean crustal growth

Opinions vary regarding the time at which plate tectonics started operating on Earth (Condie and Benn, 2006). A few authors opined that some form of horizontal tectonics (plate tectonics) operated during the Eoarchaean (Nutman et al., 2002; Shirey et. al., 2008 Komiya et al., 2015) or even Hadean (Maruyama et al., 2016). Some others argue that mantle plume related vertical tectonics was the dominant process of crust formation before the Mesoarchaean (Smithies et al., 2009; Van Kranendonk et al., 2015). Recent investigations into the global fine-grained sediment Nd isotope, and detrital zircon O and Hf isotope dataset suggest a marked decrease in rate of continental growth at ~3Ga, which is attributed to the onset of subduction-driven plate tectonics and consequent higher rate of destruction of continental crust (Næraa et al., 2012; Dhuime et al., 2017). The period from 3.0 to 2.5 Ga is marked by a distinct change in the bulk composition of continental crust from mafic to felsic (Tang et al., 2016), appearance of eclogitic diamonds (Shirey and Richardson, 2011), and increased production and diversification of granitoids (Laurent et al., 2014; Halla et al., 2017). These changes are linked to the growing importance of subduction and crust-mantle interaction.

Late Neoarchaean (2.7–2.5 Ga) greenstone belts host diverse types of volcanic and sedimentary rocks which provide significant insights into the geodynamic processes. Komatiites, oceanic plateau basalts, flood basalts, giant dyke swarms and large layered intrusions have been considered as proxies for mantle plume activity (Condie, 2001;

ACCEPTED MANUSCRIPT

Tomlinson et al., 2001; Dostal and Mueller, 2013). On the other hand, many workers interpret various tholeiitic, calc-alkaline to alkaline, mafic to felsic volcanic rocks as product of processes similar to those occurred in post-Archaean subduction zones or continental rifts (Polat and Kerrich, 2001, 2006; Wyman and Kerrich, 2009; Manikyamba and Kerrich, 2012). The relative contribution of the different processes (subduction vs. plume) in the origin of Neoarchaean crust is, however, still debated. The different types of volcanic rocks within the Veligallu greenstone belt represent a diversity of geodynamic processes. While the tholeiitic basalts and felsic volcanic rocks are linked to arc-related processes, the komatiites-komatiite basalts-ferropicrites are related to mantle plume. Such association can best be interpreted in a combined plume-arc plume model. Many of the Neoarchaean greenstone belts display coexistence of such rock associations, which indicate that interplay between mantle plume and plate tectonics was an important mechanism of crustal growth (Hollings et al., 1999; Puchtel et al., 1999; Wyman and Kerrich, 2009, 2010). This model has been contested by some workers (Bedard, 2006; Barnes and Van Kranendonk, 2014), on the basis of the fact that there may not be enough space for the mantle plume which may have large diameter (1000s of km). Wyman (2017) envisages smaller Neoarchaean plumes derived from shallow mantle depth to reconcile this problem. This is consistent with the evolution of the eastern Dharwar craton where several Neoarchaean greenstone belts host both the presumed plume-related and arc-related rock assemblages (Manikyamba et al., 2008, 2009, 2017, Manikyamba and Kerrich, 2012).

8. Conclusions

The Neoarchaean Veligallu greenstone belts contains various type of volcanic rocks which track the crustal evolutionary history of the terrane. Initially, a tholeiitic basalt was generated at ~2.67 Ga from a slightly depleted shallow mantle (ε_{Ndt} = +0.6 to +1.1) possibly within an incipient oceanic arc. As the arc matured, deposition of clastic sediments started with synchronous emplacement of mantle plume-derived komatiites, komatiitic basalts and ferropicrites, the latter displaying strong geochemical evidences for crustal contamination. Finally outpouring of diverse types of felsic volcanic rocks took place when the area possibly became a continental margin arc at ~2.58 Ga. The volcanic rocks testify mantle heterogeneity and the presence of older (Mesoarchaean) crust within the eastern Dharwar craton. An

ACCEPTED MANUSCRIPT

interplay between plume and arc is suggested to be an important mechanism of crustal growth during the Neoarchaean.

Acknowledgements

Constructive and insightful suggestions from J. Elis Hoffmann and an anonymous reviewer, and efficient editorial handling by Rajesh Hariharan and Guochun Zhao helped to improve the quality of the manuscript. SD acknowledges Indian School of Mines research grant FRS(13)/2010-11/AGL and Department of Science and Technology (DST), Government of India grant SR/S4/ES-503/2010(G). SP has received a research fellowship through the DST project SR/S4/ES-503/2010(G). The laboratory facilities in the Department of Applied Geology, IIT(ISM), funded through DST FIST Level II project No. SR/FST/ESII-014/2012(C), are also acknowledged. The isotope geochemistry facility at Pondicherry University was funded by the DST, Government of India. The Nordic geological ion-microporbe facility (Nordsim) is operated and financed under an arrangement with the Joint Committee of the Nordic Natural Science Research Councils (NOS-N), the Geological Survey of Finland and the Swedish Museum of Natural History. We acknowledge the help extended by Prof. M.J. Whitehouse for ion-microprobe analysis. This is Nordsim publication # X.

References

Abbott, D.H., Burgess, J., Longhi, J., Smith, W.H.F., 1994. An empirical thermal history of the Earth's upper mantle: a review of the evidence from komatiites. J. Geophys. Res. 99, 13835–13850.

Alt, J. C., 1999. Hydrothermal alteration and mineralization of oceanic crust: mineralogy, geochemistry and processes. In: Barrie, C. T., Hannington, M. D. (eds) Volcanic-Associated Massive Sulphide Deposits: Processes and Examples in Modern and Ancient Settings. Reviews in Economic Geology, Society of Economic Geologists, Littleton 8, 133–155.

Anand, R., Balakrishnan, S., 2010. Pb, Sr and Nd isotope systematics of metavolcanicrocks of the Hutti greenstone belt, Eastern Dharwar craton: constraints on age,duration of

ACCEPTED MANUSCRIPT

volcanism and evolution of mantle sources during Late Archean. J. Asian Earth Sci. 39, 1–11.

Arevalo, R.Jr., McDonough, W.F., 2010. Chemical variations and regional diversity observed in MORB. Chem. Geol. 271, 70–85.

Arndt, N.T., 1984. Magma mixing in komatiitic lavas from Munro Township, Ontario, In: Kroner, A., Hanson, G. N., Goodwin, A. M. (ed.), Archaean Geochemistry, Springer-Verlag, New York, 99–115.

Arndt, N.T., 1984. Magma mixing in komatiitic lavas from Munro Township, Ontario. In: Kroner, A., Hanson, G.N., Goodwin, G.A. (eds.), Archaean Geochemistry, 99–115, Spronger-Verlag, New York.

Arndt, N., Lesher, C.M., Barnes, S.J. 2008. Komatiite. Cambridge University Press. Cambridge. ISBN 9780 521 87474 8, 467 pp.

Balakrishnan, S., Hanson, G.N., Rajamani, V., 1990. Pb and Nd isotope constraints on the origin of high Mg and tholeiitic amphibolites, Kolar schist belt, southern India. Contrib. Mineral. Petrol. 107, 279–292.

Balakrishnan, S., Rajamani, V., Hansen, G.N., 1999. U-Pb ages of zircon and titanite from the Ramagiri area, southern India: evidence for accretionary origin of the eastern Dharwar Craton during the late Archean. J. Geol. 107, 69-86.

Barley, M.E., Krapez, B., Groves, D.I., Kerrich, R., 1998. The Late Archaean bonanza: metallogenic and environmental consequences of the interaction between mantle plumes, lithospheMric tectonics and global cyclicity. Precambrian Res. 91, 65–90.

Barley, M.E., Bekker, A., Krapez, B., 2005. Late Archean to Early Paleoproterozoic global tectonics, environmental change and the rise of atmospheric oxygen. Earth Planet. Sci. Lett. 238, 156–171.

Barnes, S.-J., Often, M., 1990. Ti-rich komatiites from northern Norway. Contrib. Mineral. Petrol. 105, 42–54.

Barnes, S.-J., Van Kranendonk M.J., 2014. Archean andesites in the east Yilgarn craton, Australia: products of plume-crust interaction? Lithosphere 6, 80–92.

Bedard, J. H., 2006. A catalytic delamination-driven model for coupled genesis of Archaean crust and subcontinental lithospheric mantle. Geochim. Cosmochim. Ac. 70, 1188–1214.

Bédard, J., H., 2013. How many arcs can dance on the head of a plume? A ‘Comment’ on: A critical assessment of Neoarchean ‘plume only’ geodynamics: Evidence from the

ACCEPTED MANUSCRIPT

Superior province, by Derek Wyman. Precambrian Res., 2012. Precambrian Res. 229, 189–197.

Bedard, J.H., Harris, L.B., Thurston, P.C., 2013. The hunting of the snArc. Precambrian Res. 229, 20–48.

Bidyananda, M., Goswami, J.N., Srinivasan, R., 2011. Pb–Pb zircon ages of Archaean metasediments and gneisses from the Dharwar craton, southern India: implications for the antiquity of the eastern Dharwar craton. J. Earth Syst. Sci. 120, 643–661.

Boynton, W.V., 1984. Geochemistry of the rare earth elements; meteorite studies. In: Henderson, P. (Ed.), Rare Earth Element Geochemistry. Elsevier, Amsterdam, pp. 63–114.

Castillo, P.R., 2012. Adakite petrogenesis. Lithos 134–135, 304–316.

Champion, D.C., Sheraton, J.W., 1997. Geochemistry and Nd isotope systematics of Archaean granites of the Eastern Goldfields, Yilgarn Craton, Australia: implications for crustal growth processes. Precambrian Res. 83, 109–132.

Chadwick, B., Vasudev, V.N., Krishna Rao, B., Hegde, G.V., 1992. The Dharwar Supergroup: Basin development and implications for late Archaean tectonic setting in western Karnataka, southern India. In: Glover, J.E., Ho, S. (Eds.) (Eds.), The Archaean Terrains, Processes and Metallogeny. University of western Australia Publication No. 22, 3–15.

Chadwick, B., Vasudev, V.N., Hegde, G.V., 2000. The Dharwar craton, southern India, interpreted as the result of Late Archaean oblique convergence. Precambrian Res. 99, 91–111.

Chadwick, B., Vasudev, V.N., Hegde, G.V., 2003. The Chitradurga schist belt and its adjacent plutonic rocks, northwest of Tungabhadra, Karnataka: A duplex in the late Archaean convergent setting of Dharwar craton. J. Geol. Soc. India 61, 645–663.

Chadwick, B., Vasudev, V.N., Hegde, G.V., Nutman, A., 2007. Structure and SHRIMP U/Pb ages of granites adjacent to the Chitradurga schist belt: implications for Neoarchaean convergence in the Dharwar craton, southern India. J. Geol. Soc. India 69, 5–24.

Champion, D.C., Sheraton, J.W., 1997. Geochemistry and Nd isotope systematics of Archaean granites of the Eastern Goldfields, Yilgarn Craton, Australia: implications for crustal growth processes. Precambrian Res. 83, 109–132.

Chardon, D., Choukroune, P., Jayananda, M., 1998. Sinking of the Dharwar basin (South India): implications for Archaean tectonics. Precambrian Res. 9, 15–39.

ACCEPTED MANUSCRIPT

Chardon, D., Jayananda, M., 2008. A 3D field perspective on deformation, flow and growth of the lower continental crust. Tectonics 27, TC1014, doi: 10.1029/2007TC002120.

Chardon, D., Peucat, J.-J., Jayananda, M., Choukroune, P., Fanning, C.M., 2002. Archean granite–greenstone tectonics at Kolar (South India): interplay of diapirism and bulk inhomogenous shortening during juvenile magmatic accretion. Tectonics 21 (3), 1016, http://dx.doi.org/10.1029/2001TC901032.

Chardon, D., Jayananda, M., Chetty, T.R.K., Peucat, J.-J., 2008. Precambrian continental strain and shear zone patterns: South Indian case. J. Geophys. Res. B: Solid Earth 113, B08402, http://dx.doi.org/10.1029/2007JB005299.

Chardon, D., Jayananda, M., Peucat, J.-J., 2011. Lateral constrictional flow of hot orogenic crust: insights from the Neoarchean of south India, geological and geophysical implications for orogenic plateaux. Geochem. Geophys. Geosyst. 12, Q02005, http://dx.doi.org/10.1029/2010GC003398.

Condie, K. C. 1998. Episodic continental growth and supercontinents: a mantle avalanche connection? Earth Planet. Sci. Lett. 163, 97–108.

Condie, K.C., 2001. Mantle plumes and their record in earth history. Cambridge University Press, Cambridge.

Condie, K.C., 2003. Incompatible element ratios in oceanic basalts and komatiites: Tracking deep mantle sources and continental growth rates with time. Geochem. Geophys. Geosyst. 4, 1–28.

Condie, K. C. 2004. Supercontinents and superplume events: distinguishing signals in the geologic record. Phys. Earth Planet. In. 146, 319–332.

Condie K.C. 2005. High field strength element ratios in Archean basalts: a window to evolving sources of mantle plumes? Lithos 79, 491 – 504.

Condie, K. C., Benn, K. 2006. Archean geodynamics: similar to or different from modern geodynamics. In: Benn, K., Mareschal, J. C., Condie, K. C. (eds) Archean Geodynamics and Environments. Geophysical Monograph Series 164, American Geophysical Union, Washington, D.C. 79, 47–59.

De Smeth, J.B., Rao, K.S., Schuiling, R.D., 1985. Gold-scheelite mineralization in the Veligallu Schist Belt, Andhra Pradesh, India. Econ. Geol. 80, 1996–2000.

DeCelles, P.G., Ducea, M.N., Kapp, P., Zandt, G., 2009. Cyclicity in Cordilleran orogenic systems. Nat. Geosci. 2, 251–257.

ACCEPTED MANUSCRIPT

Dey, 2013. Evolution of Archaean crust in the Dharwar craton: the Nd isotope record. Precambrian Res. 227, 227–246.

Dey, S., Gajapathi Rao, R., Gorikhan, R.A., Veerabhaskar, D., Sunil Kumar Kumar, M.K., 2003. Geochemistry and origin of northern Closepet Granite from Gudur-Guledagudda area, Bagalkot district, Karnataka. J. Geol. Soc. India 62, 152–168.

Dey, S., Rai, A.K., Chaki, A., 2009. Geochemistry of granitoids of Bilgi area, northern part of eastern Dharwar craton, southern India – example of transitional TTGs derived from depleted source. J. Geol. Soc. India 73, 854–870.

Dey, S., Pandey, U.K., Rai, A.K., Chaki, A., 2012. Geochemical and Nd isotope constraints on petrogenesis of granitoids from NW part of the eastern Dharwar craton: possible implications for late Archaean crustal accretion. J. Asian Earth Sci. 45, 40–56.

Dey, S., Nandy, J., Choudhary, A.K., Liu, Yongsheng, Zong, K., 2014. Origin and evolution of granitoids associated with the Kadiri greenstone belt, eastern Dharwar craton: A history of orogenic to anorogenic magmatism. Precambrian Res. 246, 64–90.

Dey, S., Nandy, J., Choudhary, A.K., Liu, Y., Zong, K., 2015. Neoarchaean crustal growth by combined arc–plume action: evidences from the Kadiri greenstone belt, eastern Dharwar craton, India. In: Roberts, N., van Kranendonk, M., Parman, S., Shirey, S., Clift, P. (Eds.), Continent Formation Through Time, 389. Geol. Soc. London Spec. Publ. , 135–163.

Dey, S., Halla, J., Kurhila, M., Nandy, J., Heilimo, E., Pal, S. 2016. Geochronology of Neoarchaean granitoids of the NW eastern Dharwar craton: implications for crust formation. Geol. Soc. London Spec. Publ. 449, 89–121.

Dhuime, B., Hawkesworth, C.J., Delavault, H., Cawood, P.A., 2017. Continental growth seen through the sedimentary record. Sediment. Geol. 357, 16–32.

Dostal, J, Mueller, W.U., 2013. Deciphering an Archean mantle plume: Abitibi greenstone belt, Canada. Gondwana Res. 23, 493–505.

Francis, D., Ludden, J., Johnstone, R., Davis, W., 1999. Picrite evidence for more Fe in Archean mantle reservoirs. Earth Planet. Sci. Lett. 167, 197–213.

Goldstein, S.L., O'Nions, R.K., Harmilton, P.J., 1984. A Sm–Nd isotopic study of atmospheric dusts and particulates from major river systems. Earth Planet. Sci. Lett. 70, 221–236.

ACCEPTED MANUSCRIPT

Goldstein, S.B., Francis, D., 2008. The Petrogenesis and Mantle Source of Archaean Ferropicrites from the Western Superior Province, Ontario, Canada. J. Petrol. 49, 1721–1753.

Grove T.L., Elkins-Tanton, L.T., Parman, S.W., Chatterjee N., Müntener, O., Gaetani, G.A., 2003. Fractional crystallization and mantle-melting controls on calc-alkaline differentiation trends. Contrib. Miner. Petrol. 145, 515–533.

GSI (Geological Survey of India), 2006. A manual of the Geology of India. Volume I, Part I: Southern part of the Peninsula. Geological Survey of India Special Publication No 77.

Halla, J., Whitehouse, M. J., Ahmad, T., Bagai, Z., 2017. Archaean granitoids: an overview and significance from a tectonic perspective. Geol. Soc. London Spec. Publ. 449, 1–18.

Hamilton, 2011. Plate tectonics began in Neoproterozoic time, and plumes from deep mantle have never operated. Lithos 123, 1–20.

Hanski, E. J., Huhma, H., Rastas, P., Kamenetsky, V. S., 2001. The Palaeoproterozoic komatiite-picrite association of Finnish Lapland. J. Petrol. 42, 855–876.

Hawkesworth, C.J., Gallagher, K., Hergt, J.M., McDermott, F.P., 1994. Destructive plate margin magmatism: Geochemistry and melt generation. Lithos 33, 169–188.

Herzberg, C., 1999, Phase equilibrium constraints on the formation of cratonic mantle, *in* Fei, Y., Bertka, C. M., Mysen, B. O. (eds.), Mantle petrology: field observations and high pressure experimentation, Houston, The Geochemical Society, 13–46.

Hoffmann, J.E., Kroner, A., Hegner, E., Viehmann, S., Xie, H., Iaccheri, L.M., Schneider, K.P., Hofmann, A., Wong, J., Geng, H., Yang, J., 2016. Source composition, fractional crystallization and magma mixing processes in the 3.48–3.43 Ga Tsawela tonalite suite (Ancient Gneiss Complex, Swaziland) – Implications for Palaeoarchaean geodynamics. Precambrian Res. 276, 43−66.

Hoffmann, J.E., Wilson, A.H., 2017. The origin of highly radiogenic Hf isotope compositions in 3.33 Ga Commondale komatiite lavas (South Africa). Chem. Geol. 455, 6−21.

Hollings, P., Wyman, D.A., Kerrich, R., 1999. Komatiite-basalt-rhyolite associations in northern Superior Province greenstone belts: significance of plume-arc interaction in the generation of protocontinental Superior Province. Lithos 46, 137−161.

Ishizuka, O., Tani, K., Reagan, M.K., Kanayama, K., Umino, S., Harigane, Y., Sakamoto, I., Miyajima, Y., Yuasa, M., Dunkley, D.J., 2011. The timescales of subduction initiation and subsequent evolution of an oceanic island arc. Earth Planet. Sci. Lett. 306, 229–240.

ACCEPTED MANUSCRIPT

Jahn B.-M., Vidal P., Tilton, G. R., 1980. Archaean mantle heterogeneity: evidence from chemical and isotopic abundances in Archaean igneous rocks. Phil. Trans. Roy. Soc. London A297, 353–364.

Jayananda, M., Martin, H., Peucat, J.J., Mahabaleshwar, B., 1995. Late Archean crust mantle interaction: geochemistry of LREE enriched mantle derived magmas. Example of the Closepet batholith, southern India. Contrib. Mineral. Petrol. 119, 314–329.

Jayananda, M., Moyen, J.-F., Martin, H., Peucat, J.-J., Auvray, B., Mahabaleshwar, B., 2000. Late Archean (2550–2520 Ma) juvenile magmatism in the Eastern Dharwar Craton, Southern India: constrains from geochronology, Nd–Sr isotopes and whole rock geochemistry. Precambrian Res. 99, 225–254.

Jayananda, M., Chardon, D., Peucat, J.-J., Capdevila, R., 2006. 2.61 Ga potassic granitesand crustal reworking in the western Dharwar craton, southern India: tectonic,geochronologic and tectonic constraints. Precambrian Res. 150, 1–26.

Jayananda, M., Kano, T., Peucat, J.-J., Channabasappa, S., 2008. 3.35 Ga komatiite volcanism in the western Dharwar craton, southern India: constraints from Ndisotopes and whole-rock geochemistry. Precambrian Res. 162, 160–179.

Jayananda, M., Banerjee, M., Pant, N. C., Dasgupta, S., Kano, T., Mahesha, N., Mahableswar, B., 2012. 2.62 Ga high-temperature metamorphism in the central part of the Eastern Dharwar Craton: implications for late Archaean tectonothermal history. Geol. J.47, 213–236.

Jayanandaa, M., Peucat, J.-J., Chardonc, D., Krishna Raod, B., Fanninge, C.M., Corfu, F. 2013a. Neoarchean greenstone volcanism and continental growth, Dharwar craton, southern India: Constraints from SIMS U–Pb zircon geochronology and Nd isotopes, Precambrian Res. 227, 55–76.

Jayananda, M., Tsutsumi, Y., Miyazaki, T., Gireesh, R.V., Kapfo, K., Tushipokla, Hidaka, H., Kano, T., 2013b. Geochronological constraints on Meso- and Neoarchean regional metamorphism and magmatism in the Dharwar craton, southern India. J. Asian Earth Sci. 78, 18–38.

Jayananda, M., Chardon, D., Peucat, J.-J., Tushipokla, Fanning, C.M., 2015. Paleo- to Mesoarchean TTG accretion and continental growth in the western Dharwar craton, Southern India: Constraints from SHRIMP U–Pb zircon geochronology, whole-rock geochemistry and Nd–Sr isotopes. Precambrian Res. 268, 295–322.

ACCEPTED MANUSCRIPT

Jayananda, M., Santosh, M., Aadhiseshan, K.R., 2018. Formation of Archean (3600–2500 Ma) continental crust in the Dharwar Craton, southern India. Earth Sci. Rev. 181, 12−42.

Jensen, L. S., 1976. A new cation plot for classifying subalkalic volcanic rocks. Ont. Div. Mines, Misc. Pap. 66, 1–21.

Kelemen, P.B., Hanghoj, K., Greene, A.R., 2014. One view of the geochemistry of subduction-related magmatic arcs, with an emphasis on primitive andesite and lower crust. Treatise on Geochemistry 4, 749–806.

Kerrich, R., Polat, A., Wyman, D., 1999. Trace element systematics of Mg- to Fe-tholeiitic basalt suites of the Superior Province: Implications for Archean mantle reservoirs and greenstone belt genesis. Lithos 46, 163–187.

Khanna, T.C., Sesha Sai, V.V., Bizimis, M., 2015. Petrogenesis of basalt–high-Mg andesite–adakite in the Neoarchean Veligallu greenstone terrane: geochemical evidence for a rifted back-arc crust in the eastern Dharwar craton, India. Precambrian Res. 258, 260–277.

Khanna, T.C., Sesha Sai, V.V., Bizimis, M., Krishna, A.K., 2016. Petrogenesis of ultramafics in the Neoarchean Veligallu greenstone terrane, eastern Dharwar craton, India: Constraints from bulk-rock geochemistry and Lu-Hf isotopes. Precambrian Res. 285, 186–201.

Komiya, T., Yamamoto, S., Aoki, S., Sawaki, Y., Ishikawa, A., Tashiro, T., Koshida, K., Shimojo, M., Aoki, K., Collerson, K.D., 2015. Geology of the Eoarchean, > 3.95 Ga, Nulliak supracrustal rocks in the Saglek Block, northern Labrador, Canada: The oldest geological evidence for plate tectonics Tectonophysics 662, 40–66.

Krogstad, E.J., Hanson, G.N., Rajamani, V., 1995. Sources of continental magmatism adjacent to the late Archaean Kolar suture zone, south India: distinct isotopic and elemental signatures of two late Archaean magmatic series. Contrib. Mineral. Petrol. 122, 159–173.

Kumar, Anil, Bhaskar Rao, Y.J., Sivaraman, T.V., Gopalan, K., 1996. Sm–Nd ages of Archean metavolcanics of the Dharwar Craton, South India. Precambrian Res. 80, 205–216.

Laurent, O., Martin, H., Moyen, J-.F., Doucelance, R., 2014. The diversity and evolution of late-Archean granitoids: evidence for the onset of “modern-style” plate tectonics between 3.0 and 2.5 Ga. Lithos 208, 205–235.

ACCEPTED MANUSCRIPT

Lee, C.T-A., Anderson, D.L., 2015. Continental crust formation at arcs, the arclogite "delamination" cycle, and one origin for fertile melting anomalies in the mantle. Sci. Bull. 60, 1141–1156.

Lehtonen, E., Heilimo, E,. Halkoaho, T., Käpyaho, A., Hölttä, P., 2016. U-Pb geochronology of Archaean volcanic-sedimentary sequences in the Kuhmo greenstone belt, Karelia Province - Multiphase volcanism from Meso- to Neoarchaean and a Neoarchaean depositional basin? Precambrian Res. 275, 48-69.

Manikyamba, C., Kerrich, R., 2011. Geochemistry of alkaline- and associated High-Mg basalts from the 2.7 Ga Penakacherla Terrane, Dharwar Craton, India: an Archean depleted mantle-OIB array. Precambrian Res. 188, 104–122.

Manikyamba, C., Kerrich, R. 2012. Eastern Dharwar craton, India: continental lithosphere growth by accretion of diverse plume and arc terranes. Geosci. Front. 3, 225–240.

Manikyamba, C., Kerrich, R., Khanna, T. C., Krishna, A. K., Satyanarayanan, M., 2008. Geochemical systematics of komatiite–tholeiite and adakite–arc basalt associations: the role of a mantle plume and convergent margin in formation of the Sandur Superterrane, Dharwar Craton, India. Lithos 106, 155–172.

Manikyamba, C., Kerrich, R., Khanna, T.C., Satyanarayanan, M., Krishna, A.K., 2009. Enriched and depleted arc basalts, with high-Mg andesites and adakites: a potential paired arc-back arc of the 2.7 Ga Hutti greenstone terrane, India. Geochim. Cosmochim. Ac. 73, 1711–1736.

Manikyamba, C., Ganguly, S., Santosh, M., Singh, M.R., Saha, A., 2015. Arc-nascent back-arc signature in metabasalts from the Neoarchaean Jonnagiri greenstone terrane, Eastern Dharwar Craton, India. Geol. J. 50, 651–669.

Manikyamba, C., Ganguly, S., Santosh, M., Subramanyam, S.V., 2017. Volcano-sedimentary and metallogenic records of the Dharwar greenstone terranes, India: Window to Archean plate tectonics, continent growth, and mineral endowment. Gond. Res. 50, 38–66.

Martin, H., Smithies, R.H., Rapp, R., Moyen, J.-F., Champion, D., 2005. An overview of adakite, tonalite-trondhjemite-granodiorite (TTG), and sanukitoids: relation-ships and some implications for crustal evolution. Lithos 79, 1–24.

Maruyama, S., Santosh, M., Azuma, S., 2016. Initiation of plate tectonics in the Hadean: Eclogitization triggered by the ABEL Bombardment. Geosci. Front., in press, doi: 10.1016/j.gsf.2016.11.009 .

ACCEPTED MANUSCRIPT

Masters, R. L., Argue, J. J., 2005. Regional scale fluid flow and element mobility in Barrow's metamorphic zones, Stonehaven, Scotland. Contrib. Mineral. Petrol. 150, 1–18.

Maya, J.M., Bhutani, R., Balakrishnan, S., Sandhya, S.R., 2016. Petrogenesis of 3.15 Ga old Banasandra komatiites from the Dharwar craton, India: Implications for early mantle heterogeneity. Geosci. Front. 8, 467–489.

Meen, J.K., Roggers, J.J.W., Fullager, P.D., 1992. Lead isotopic compositions of the Western Dharwar Craton, southern India: evidence for distinct middle Archaean Terranes in a late Archaean Craton. Geochim. Cosmochim. Ac. 56, 2455–2470.

Mikkola, P., Huhma, H., Heilimo, E., Whitehouse, M.J., 2011. Archean crustal evolution of the Suomussalmi district as part of the Kianta Complex, Karelia: Constraints from geochemistry and isotopes of granitoids. Lithos 125, 287–307.

Milidragovic, D., Francis, D., 2016. Ca. 2.7 Ga ferropicritic magmatism: A record of Fe-rich heterogeneities during Neoarchean global mantle melting. Geochim. Cosmochim. Ac. 185, 44–63.

Milidragovic, D., Francis, D., Weis, D., Constantin, M., 2014. Neoarchean (c. 2.7 Ga) plutons of the Ungava craton, Quebec, Canada: Parental magma compositions and implications for Fe-rich mantle source region. J. Petrol. 55, 2481–2512.

Mole, D.R., Fiorentini, M.L., Thebaud, N., Cassidy, K.F., McCuaig, T.C., Kirkland, C.L., Romano, S.S., Doublier, M.P., Belousova, E.A., Barnes, S.J., Miller, J., 2014. Archean komatiite volcanism controlled by the evolution of early continents. PNAS 111, 10083–10088.

Moyen, J. F. 2010. High Sr/Y and La/Yb ratios: the meaning of the 'adakitic signature'. Lithos 112, 556–574.

Moyen, J.-F., Martin, H., Jayananda, M., Auvray, B., 2003. Late Archaean granites: a typology based on the Dharwar Craton (India). Precambrian Res. 127, 103–123.

Mungall, J.E., Crustal contamination of picritic magmas during transport through dikes: the Expo Intrusive Suite, Cape Smith Fold Belt, New Quebec. J. Petrol. 48, 1021–1039.

Næraa, T., Scherste´n, A., Rosing, M.T., Kemp, A.I.S., Hoffmann, J.E., Kokfelt, T.F., Whitehouse, M.J., 2012. Hafnium isotope evidence for a transition in the dynamics of continental growth 3.2Gyr ago. Nature 485, 627–631.

Naqvi, S.M., Manikyamba, C., Ganeshwara Rao, T., Subba Rao, D.V., Ram Mohan, M, Srinivasa Rama, D., 2002. Geochemical and isotopic constraints of Neoarchaeanfossil

ACCEPTED MANUSCRIPT

plume for evolution of volcanic rocks of Sandur greenstone belt, India. J. Geol. Soc. India 60, 27–56.

Naqvi, S. M., Khan, R. M. K., Manikyamba, C., Ram Mohan, M., Khanna, T. C. 2006. Geochemistry of the NeoArchaean high-Mg basalts, boninites and adakites from the Kushtagi–Hungund greenstone belt of the Eastern Dharwar Craton (EDC); implications for the tectonic setting. J. Asian Earth Sci. 27, 25–44.

Nelson, S.A., Livieres, R.A., 1986. Contemporaneous calc-alkaline and alkaline volcanism at Sanganguey Volcano, Nayarit, Mexico. Geol. Soc. Am. Bull. 97, 798–808.

Niu, Y., M. Regelous, J. I. Wendt, R. Batiza, O'Hara, M. J., 2002. Geochemistry of near-EPR seamounts: Importance of source vs. process and the origin of enriched mantle component, Earth Planet. Sci. Lett. 199, 327–345.

Nutman, A. P., Friend, C.R. L., Bennett, V. C., 2002. Evidence for 3650–3600 Ma assembly of the northern end of the Itsaq Gneiss Complex, Greenland: implication for early Archaean tectonics. Tectonics, 21, http://dx.doi.org/10.1029/2000TC001203.

Parat, F., Dungan, M.A., Lipman, P.W., 2005. Contemporaneous Trachyandesitic and Calc-alkaline Volcanism of the Huerto Andesite, San Juan Volcanic Field, Colorado, USA. J. Petrol. 46, 859–891.

Pearce, J. A., 1996. A User's Guide to Basalt Discrimination Diagrams. In: Wyman D. A. (ed) Trace Element Geochemistry of Volcanic Rocks: Applications for Massive Sulphide Exploration. Geological Association of Canada, Short Course Notes 12, 79–113.

Pearce, J.A., 2008. Geochemical fingerprinting of oceanic basalts with applications to ophiolite classification and the search for Archaean oceanic crust. Lithos 100, 14-48.

Pearce, J.A., Peate, D.W., 1995. Tectonic implications of the compositions of volcanic arc magmas. Annu. Rev. Earth Planet. Sci. 23, 251–285.

Pease, V., Percival, J., Smithies, H., Stevens, G. 2008. When did plate tectonics begin? Evidence from the orogenic record. In: Condie, K. C., Pease, V. (eds) When Did Plate Tectonics Begin on Planet Earth? Geol. Soc. Spec. Pap. 340, 199–228.

Perfit, M.R., Gust, D.A., Bence, A.E., Arculus, R.J., Taylor, S.R., 1980. Chemical Characteristics of Island-Arc Basalts - Implications for Mantle Sources. Chem. Geol. 30, 227–256.

ACCEPTED MANUSCRIPT

Perring, C.S., Barnes, S. J., Hill, R.E.T., 1996, Geochemistry of komatiites from Forrestania, Southern Cross Province, Western Australia: Evidence for crustal contamination. Lithos 37, 181−197.

Peucat, J.J., Mahabaleswar, B., Jayananda, M., 1993. Age of younger tonalitic mag-matism and granulitic metamorphism in the South Indian transition zone(Krishnagiri area); comparison with older Peninsular Gneisses from the Gorur-Hassan area. J. Metamorph. Geol. 11, 879–888.

Peucat, J.J., Jayananda, M., Chardon, D., Capdevila, R., Fanning, C.M., Paquette, J.-L., 2013. The lower crust of the Dharwar Craton, Southern India: Patchwork of Archean granulitic domains. Precambrian Res. 227, 4–29.

Polat, A., Hofmann, A. W. 2003. Alteration and geochemical patterns in the 3.7–3.8 Ga Isua greenstone belt, West Greenland. Precambrian Res. 126, 197–218.

Polat, A., Kerrich, R. 2001. Geodynamic processes, continental growth, and mantle evolution recorded in late Archean greenstone belts of the southern Superior Province, Canada. Precambrian Res. 112, 5–25.

Polat, A., Kerrich, R. 2006. Reading the geochemical fingerprints of Archean hot subduction volcanic rocks: evidence for accretion and crustal recycling in a mobile tectonic regime. In: Benn, K., Mareschal, J.-C., Condie, K. C. (eds) Archean Geodynamics and Environments. Geophysical Monograph Series 164, American Geophysical Union, Washington D.C., 189–213.

Polat, A., Kerrich, R., Windley, B.F., 2009. Archean crustal growth processes in the southern Superior Province and southern West Greenland: geodynamic and magmatic constraints. In: Cawood, P. A., Kröner, A. (Eds.), Accretionary Orogens in Space and Time, Geological Society of London, Special Publication 318, 155-191.

Puchtel, I.S., Haase, K.M., Hofmann, A.W., Chauvel, C., Kulikov, V.S., Garbe-Schonberg, C.-D., Nemchin, A.A., 1997. Petrology and geochemistry of crustally contaminated komatiitic basalts from the Vetreny Belt, southeastern Baltic Shield: Evidence for an early Proterozoic mantle plume beneath rifted Archean continental lithosphere. Geochim. Cosmochim. Ac. 61, 1205–1222.

Puchtel, S., Hofmann, A.W., Amelin, Y.V., Garbe-Schonberg, C.D., Samsonov, A.V., Shchipansky, A.A., 1999. Combined mantle plume–island arc model for the formation of the 2.9 Ga Sumozero-Kenozero greenstone belt, SE Baltic Shield: isotope and trace element constraints. Geochim. Cosmochim. Ac. 63, 3579–3595.

ACCEPTED MANUSCRIPT

Ramam, P.K., Murty, V.N., 1997. Geology of Andhra Pradesh. Geological Society of India, Bangalore, pp. 1–245.

Ram Mohan, M., Piercey, S.J., Kamber, B.S., Srinivasa Sarma, D., 2013. Subductionrelated tectonic evolution of the Neoarchean eastern Dharwar Craton, southernIndia: new geochemical and isotopic constraints. Precambrian Res. 227, 204–226.

Rajamani, V., Shivkumar, K., Hanson, G. N., Shirey, S. B., 1985. Geochemistry and petrogenesis of amphibolites, Kolar Schist belt, South India: evidence for komatiitic magma derived by low percentages of melting in the mantle. J. Petrol. 26, 92–123.

Rajamani, V., Shirey, S. B., Hanson, G. N., 1989. Fe-rich Archean tholeiites derived from melt-enriched mantle sources: evidence from the Kolar Schist belt, South India. J. Geol. 97, 487–501.

Rajamanickam, M., Balakrishnan, S., Bhutani, R., 2014. Rb–Sr and Sm–Nd isotope systematics and geochemical studies on metavolcanic rocks from Peddavura greenstone belt: Evidence for presence of Mesoarchean continental crust in easternmost part of Dharwar Craton, India. J. Earth Syst. Sci. 123, 989–1011.

Reddy, S.M., Evans, D.A.D., 2009. Palaeoproterozoic supercontinents and global evolution: correlations from core to atmosphere. In: Reddy, S.M., Mazumder, R., Evans, D. A. D., Collins, A. S. (eds), Palaeoproterozoic Supercontinents and Global Evolution. Geol. Soc. London Spec. Publ. 323, 1–26.

Richards, J. P., Kerrich, R. 2007. Adakite-like rocks: their diverse origins and questionable role in metallogenesis. Econ. Geol. 102, 537–576.

Rogers, A.J., Kolb, J., Meyer, F.M., Armstrong, R.A., 2007. Tectonomagmatic evolution of the Hutti-Maski greenstone belt, India: constrained using geochemical and geochronological data. J. Asian Earth Sci. 31, 55–70.

Ross, P.-S., Bedard, J.H., 2009. Magmatic affinity of modern and ancient subalkaline volcanic rocks determined from trace-element discrimination diagrams. Can. J. Earth Sci. 46, 823–839.

Rudnick, R.L., 1995. Making continental crust. Nature 378, 415–445.

Rudnick, R.L., Gao, S., 2003. The composition of the continental crust. In: Treatise on Geochemistry - The Crust. Rudnick, R.L., Holland, H.D., Turekian, K.K. (Editors), Elsevier, Oxford. 1–64.

Said, N., Kerrich, R., Cassidy, K., Champion, D.C., 2012. Characteristics and geodynamic setting of the 2.7 Ga Yilgarn heterogeneous plume and its interaction with continental

ACCEPTED MANUSCRIPT

lithosphere: evidence from komatiitic basalt and basalt geochemistry of the Eastern Goldfields Superterrane. Aust. J. Earth Sci. 59, 737-763.

Sarma, D.S., McNaughton, N.J, Fletcher, I.R., Groves, D.I., Ram Mohan, M., Balaram, V., 2008. The timing of gold mineralization of Hutti gold deposit, Dharwar Craton, South India. Econ. Geol. 103, 1715–1727.

Salters, V.J.M., Stracke, A., 2004. Composition of the depleted mantle. Geochem. Geophy. Geosy. 5, doi: 10.1029/2003GC000597.

Schmitz, M.D., Bowring, S.A., Southwick, D.L., Boerboom, T.J., Wirth, K.R., 2006. High-precision U-Pb geochronology in the Minnesota River Valley subprovince and its bearing on the Neoarchean to Paleoproterozoic evolution of the southern Superior Province. Geology 118, 82–93.

Shirey, S.B., Kamber, B.S., Whitehouse, M.J., Mueller, P.A., Basu, A.R., 2008. A review of the isotopic and trace element evidence for mantle and crustal processes in the Hadean and Archean: implications for the onset of plate tectonic subduction. In: Condie, K.C., and Pease, V. (eds.), When Did Plate Tectonics Begin on Planet Earth?: Geological Society of America Special Paper 440, 1–29, doi: 10.1130/2008.2440(01).

Shirey, S.B., Richardson, S.H., 2011. Start of the Wilson cycle at 3 Ga shown by diamonds from subcontinental mantle. Science 333, 434−436.

Smithies, R.H., Champion, D.C., van Kranendonk, M.J., 2009. Formation of continental crust through infracrustal melting of enriched basalt. Earth Planet. Sc. Lett. 281, 298–306.

Sobolev, A.V., Asafov, E.V., Gurenko, A.A., Arndt, N.T., Batanoval, V.G., Portnyagin, M.V., Garbe-Schönberg, D., Krasheninnikov, S.P., 2016. Komatiites reveal a hydrous Archaean deep-mantle reservoir. Nature 531, 628–632.

Sparks, R.J.S., 1986. The role of crustal contamination in magma evolution through geological time. Earth Planet. Sci. Lett. 78, 211–223.

Stacey, J.S., Kramers, J.D., 1975. Approximation of terrestrial lead isotope evolution by a two stage model. Earth Planet. Sci. Lett. 26, 207–221.

Stein, M., Hofmann, A.W., 1994. Mantle plumes and episodic crustal growth. Nature 372, 63–68.

Stone, W. E., Crocket, J. H., Dickin, A. P., Fleet, M. E., 1995. Origin of Archean ferropicrites: geochemical constraints from the Boston Creek Flow, Abitibi greenstone belt, Ontario, Canada. Chemical Geology 121, 51–71.

ACCEPTED MANUSCRIPT

Subba Rao, K., Sesha Sai, V.V., 2012. Exploration for gold in the Tellakonda block of Veligallu greenstone belt, Kadapa district, Andhra Pradesh. Progress Report for the Field Seasons: 2010-12, Code No. ME/SR/AP/2010/016, Geological Survey of India, Hyderabad, p. 49.

Sun, S.-S., McDonough, W. F., 1989. Chemical and isotopic systematics of oceanic basalts: implications for mantle composition and processes. In: Sounders, A. D., Norry, M. J. (eds) Magmatism in the Ocean Basins. Geol. Soc. London Spec. Publ. 42, 313–345.

Swami Nath, J., Ramakrishnan, M. (Eds.), 1981. Early Precambrian Supracrustals of Southern Karnataka, Mem. Geol. Surv. India 112, p. 352.

Szilas, K., Hoffmann, J.E., Scherstén, A., Rosing, M.T., Windley, B.F., Kokfelt, T.F., Keulen, N., van Hinsberg, V.J., Næraa, T., Frei, R., Münker, C., 2012. Complex calc-alkaline volcanism recorded in Mesoarchaean supracrustal belts north of Frederikshåb Isblink, southern West Greenland: Implications for subduction zone processes in the early Earth. Precambrian Res. 208−211, 90–123.

Szilas, K., Tusch, J., Hoffmann, J.E., Garde, A.A., Münker, C., 2016. Hafnium isotope constraints on the origin of Mesoarchaean andesites in southern West Greenland, North Atlantic Craton. Geol. Soc. London Spec. Publ. 449, 19–38.

Tang, M., Chen, K., Rudnick, R.L., 2016. Archean upper crust transition from mafic to felsic marks the onset of plate tectonics. Science 351, 372−375.

Tatsumi, Y., 2000. Continetal crust formation by crustal delamination in subduction zones and complementary accumulation of the enriched mantle I component in the mantle. Geochem. Geophy. Geosy. 1, 2000GC000094.

Tomlinson, K. Y., Condie, K. C., 2001. Archean mantle plumes: evidence from greenstone belt geochemistry. In: Ernst, R. E., Buchan, K. L. (eds) Mantle plumes: their identification through time. Geol. Soc. Spec. Pap. 352, 341–357.

Van Kranendonk, M. J., Smithies, R.H., Griffin, W.L., Huston, D.L., Hickman, A.H., Champion, D.C., Anhaeusser, C.R., Piranjo, F., 2015. Making it thick: a volcanic plateau origin of Palaeoarchean continental lithosphere of the Pilbara and Kaapvaal cratons. In: Roberts, N. M. W., Van Kranendonk, M., Parman, S., Shirey, S., Clift, P. D. (eds), Continent Formation Through Time. Geol. Soc. London Spec. Publ. 389, 83–111.

Vrevsky, A., Krimsky, R., Svetov, S., 1996. Rare earth and isotopic (Nd, O) heterogeneity of the Archaean mantle, Baltic Shield. In: Brewer, T.S. (ed), Precambrian crustal evolution in the North Atlantic Region. Geol. Soc. London Spec. Publ. 112, 43–53.

ACCEPTED MANUSCRIPT

Wang, W., Liu, S., Santosh, M., Wang, G., Bai, X., Guo, R., 2015. Neoarchean intra-oceanic arc system in the Western Liaoning Province: Implications for Early Precambrian crustal evolution in the Eastern Block of the North China Craton. Earth-Sci. Rev. 150, 329–364.

Winchester, J.A., Floyd, P.A., 1977. Geochemical discrimination of different magma series and their differentiation products using immobile elements. Chem. Geol. 20, 325–343.

Wyman, D.A., 2013. A critical assessment of Neoarchean "plume only" geodynamics: evidence from the Superior Province. Precambrian Res. 229, 3–19.

Wyman, D.A., Hollings, P., Biczok, J., 2011. Crustal evolution in a cratonic nucleus: Granitoids and felsic volcanic rocks of the North Caribou Terrane, Superior Province Canada. Lithos 123, 37–49.

Wyman, D., Kerrich, R., 2009. Plume and arc magmatism in the Abitibi subprovince: Implications for the origin of Archean continental lithospheric mantle. Precambrian Res. 168, 4–22.

Wyman, D., Kerrich, R., 2010. Mantle plume – volcanic arc interaction: consequences for magmatism, metallogeny, and cratonization in the Abitibi and Wawa subprovinces, Canada. Can. J. Earth Sci. 47, 565–589.

Zachariah, J.K., Rajamani, V., Hanson, G.N., 1997. Petrogenesis and source characteristics of metatholeiites from the Archean Ramagiri schist belt, eastern part of Dharwar craton, India. Contrib. Mineral. Petr. 129, 87–104.

Figure Captions

Fig. 1. Geological map of the Dharwar craton (modified after Chardon et al., 2008) showing the location of the Veligallu greenstone belt. Other greenstone/schist belts: Bb – Bababudan, C – Chitradurga, G – Gadwal, H – Hutti, HK – Hungund-Kushtagi, Hn – Holenarasipur, K – Kolar, Ka – Kadiri, Ku – Kudremukh, N – Nuggihalli, P – Penakacherla, R – Ramagiri, Rc – Raichur, S – Sandur, Sg – Sargur, Sh – Shimoga. CSZ – Chitradurga shear zone. Inset: EG – Eastern Ghats Mobile Belt, SGT – Southern Granulite Terrain.

Fig. 2. Geological map of the Veligallu greenstone belt and associated granitoids showing the location of samples. The sample numbers are shown without prefix. Samples dated by zircon U–Pb method are marked by red stars.

Fig. 3. Field and petrographic features of Veligallu greenstone belt: (a) Pillows (arrowed) in southern mafic rock, 2.8 km NE of Tamblapalle. (b) Photomicrograph showing association of

ACCEPTED MANUSCRIPT

hornblende and plagioclase with minor quartz and opaques in southern mafic rock. The foliation defined by parallel alignment of amphibole grains. Crossed nicols (XPL). (c) Coarse-grained gabbro showing layering (indicated by the yellow dashed line). 3.5 km N of Tamblapalle. (d) Photomicrograph of coarse-grained gabbro consisting of hornblende (altering to tremolite-actinolite) with interstitial plagioclase grains. Plane polarized light (PPL). (e) Photomicrograph showing intergranular texture of gabbro in which subhedral uralised augite grains occupy the interstitial spaces between sericitised plagioclase laths. XPL. (f) Bands of ultramafic rocks (dark) intercalated with quartz-muscovite schist (light-coloured). ~10 km SW of Veligallu. (g) Photomicrograph showing association of tremolite-actinolite and hornblende in the northern ultramafic rock. XPL. (h) Banded felsic volcanic rock (adakite), 4.8 km SE of Tamblapalle. (i) Photomicrograph showing association of plagioclase, quartz and hornblende in felsic volcanic rock. (j) Photomicrograph showing overall texture of felsic volcanic rock consisting of quartz, plagioclase and chlorite. Parallel alignment of chlorite defines a distinct foliation in the rock. Relict hornblende is being replaced by chlorite in the upper centre. XPL. A – augite, C – chlorite, H – hornblende, P – plagioclase, Q – quartz, T- tremolite-actinolite.

Fig. 4. (a) Nb/Y vs. Zr/Ti (Winchester and Floyd, 1977 as modified by Pearce (1996) (b) Zr/Y vs. Th/Yb (Ross and Bedard. 2009) classification of Veligallu metaigneous rocks.

Fig. 5. Variation of major and trace elements with respect to MgO in Veligallu metaigneous rocks. The Ni and Cr concentrations are plotted in logarithmic scale due to their large variation. The Veligallu ultramafic rocks of Khanna et al. (2015), and basalts and felsic volcanic rocks (high-Mg andesites and adakites) of Khanna et al. (2016) presumably correspond to komatiite, southern basalt and felsic volcanic rocks, respectively, of the present work. They are plotted in grey with the same symbols.

Fig. 6. Chondrite-normalized REE (Boynton, 1984) and primitive mantle-normalized (Sun and McDonough, 1989) trace element plots of the Veligallu metaigneous rocks: (a, b) southern basalts; (c, d) northern mafic-ultramafic rocks (komatiite, komatiitic basalts and ferropicrites); (e, f) felsic volcanic rocks. Note that among the northern mafic-ultramafic rocks, samples VB273, VB288 and VB294 are recognised as ferropicrites. Abbreviations: Sed high and sed low - the upper and lower compositional envelopes of the Veligallu sedimentary rocks. VGG - Veligallu granitoid gneiss (unpublished data of the authors). UCC and LCC - average upper and lower continental crust respectively - (Rudnick and Gao, 2003).

ACCEPTED MANUSCRIPT

The Veligallu ultramafic rocks of Khanna et al. (2015), and basalts and felsic volcanic rocks (high-Mg andesites and adakites) of Khanna et al. (2016) presumably correspond to komatiite, southern basalt and felsic volcanic rocks, respectively, of the present work. They are plotted as grey background in the respective diagrams.

Fig. 7. Veligallu metaigneous rocks rocks on Nb/Yb vs. Th/Yb space (after Pearce, 2008). Data source: average NMORB and OIB - Sun and McDonough (1989); average E-MORB - Niu et al. (2002). The Veligallu ultramafic rocks of Khanna et al. (2015), and basalts and felsic volcanic rocks (high-Mg andesites and adakites) of Khanna et al. (2016) presumably correspond to komatiite, southern basalt and felsic volcanic rocks, respectively, of the present work. They are plotted in grey with the same symbols.

Fig. 8. Al_2O_3/TiO_2 vs. Gd_N/Yb_N ratio plot of the Veligallu metaigneous rocks. The subscript 'N' denotes chondrite-normalized values (Boynton, 1984). The Veligallu ultramafic rocks of Khanna et al. (2015), and basalts and felsic volcanic rocks (high-Mg andesites and adakites) of Khanna et al. (2016) presumably correspond to komatiite, southern basalt and felsic volcanic rocks, respectively, of the present work. They are plotted in grey with the same symbols.

Fig. 9. Zircons from Veligallu andesite sample VAV127: (a) Representative back-scattered electron (BSE) images. Small circles shows SIMS analysis spots (numbers corresponding to Table 2). The black area outside each zircon is background. (b) Concordia diagram for U–Pb dating. The error ellipses drawn at 2σ level.

Fig. 10. Sm-Nd whole-rock isochron for the southern basalts of the Veligallu greenstone belt. The decay constant used is $6.54\times10^{-12}a^{-1}$.

Fig. 11. HFSE ratio plots for the metaigneous rocks of the Veligallu belt. (a) Nb/Yb vs. Zr/Yb (fields after Pearce and Peate, 1995) and (b) Zr/Y vs. Nb/Y (after Condie, 2005). Data source: average primitive mantle, NMORB and OIB - Sun and McDonough (1989); average E-MORB - Niu et al. (2002); Upper and total continental crust - Rudnick and Gao (2003). Enriched mantle component from Condie (2005). Basalts plotting in the non-plume source field are derived either from shallow depleted source or subduction zone, or formed from plume sources followed by contamination with continental crust or subcontinental lithosphere.

ACCEPTED MANUSCRIPT

Fig. 12. Y vs. Zr/Y plots for the Veligallu metaigneous rocks. Data source: Upper, lower and total continental crust - Rudnick and Gao (2003); primitive mantle - Sun and McDonough (1989); depleted mantle (source of MORB) - Salters and Stracke (2004).

Fig. 13. $^{147}Sm/^{144}Nd$ vs. initial εNd plot for the Veligallu metaigneous rocks. Data source: Granitic gneiss - Jayananda et al. (2000); Depleted mantle and chondrite - Goldstein et al. (1984); Veligallu sedimentary rocks - unpublished data of the authors.

Table Captions

Table 1. Major (wt%) and trace (ppm) element compositions of metaigneous rocks of the Veligallu greenstone belt, eastern Dharwar craton, India.

Table 2. U-Pb isotopic data of zircons from the andesite sample VAV127.

Table 3. Sm-Nd isotope data on metaigneous rocks of the Veligallu greenstone belt, eastern Dharwar craton, India.

Appendix 1: Analytical Techniques

Whole-rock major and trace element analysis

The whole-rock samples were analyzed for major and trace elements in the laboratory of Actlabs, Ontario, Canada using their analytical package 'code 4LITHO' (data in Table 1). Powered samples weighing 200 mg along with standards were fused using a lithium metaborate/tetraborate flux and then totally dissolved using 5% HNO_3. Major elements, Ba, Sr, Y, Zr, Be, Sc and V were analysed using an ICP (Varian 735 ICP-OES) and all other elements by an ICP-MS (ELAN 9000). Loss on ignition was determined by heating powdered samples for 2 hours at 1050 ^{0}C. Nineteen international rock standards of variable compositions were analysed simultaneously and the values obtained for them are available with the corresponding author on request. Analytical uncertainties depend on the concentration of elements. In general, the uncertainties are within 2% for SiO_2, Al_2O_3, CaO and K_2O, within 4% for Fe_2O_3, MnO, MgO, Na_2O and within 5% for P_2O_5 and TiO_2. Uncertainties for the trace elements are usually within 10%. Further details of analytical techniques are given in http://www.actlabs.com/.

ACCEPTED MANUSCRIPT

Zircon U-Pb dating

The zircons were separated using standard procedures including crushing (in iron mortar and pestle), sieving (375 to 75 micron), tabling, heavy liquid separation (bromoform and methylene iodide) and magnetic separation. The grains were hand-picked under a binocular microscope and mounted in epoxy. For imaging and U-Pb analyses the sample mount was gold-coated. The zircon images were obtained at the Geological Survey of Finland with a Jeol JSM-5900LV scanning electron microscope in a back-scattered electron detection mode. The accelerating voltage was 20 kV and beam current was 54 mA. Working distance between the filament and the sample surface was 11 mm.

The ion microprobe analyses were performed using the Cameca IMS 1280 of the NORDSIM laboratory at the Swedish Museum of Natural History, Stockholm (data in Table 2). The spot diameter for the ~4.5 nA primary O_2^- ion beam was ~20 µm and oxygen flooding in the sample chamber was used to increase the production of Pb^+ ions. Three counting blocks, each including four cycles of the Zr, Hf (for mass calibration optimization), Pb, Th, and U species of interest, were measured from each spot. Sequential mono-collection mode with an electron multiplier was used. The mass resolution (M/ΔM) was 5300 (10%). The data were calibrated against a zircon standard (91,500; Wiedenbeck et al., 1995) and corrected for modern common Pb (T = 0; Stacey and Kramers, 1975). The procedure was essentially similar to that described in detail by Whitehouse et al. (1999) and Whitehouse and Kamber (2005).

Whole-rock Nd isotope analysis

The whole-rock samples were digested through acid digestion technique using double sub-boiled distilled HF, HNO_3 and HCl acids in a 7 ml Savillex® vial till a clear sample solution was obtained. Further the digested clear solution was dried and the residue was dissolved in 5ml of 2N HCl. About one third of the digested samples were spiked with ^{152}Sm and ^{150}Nd enriched spike solution for the determination of concentration of Sm and Nd by isotope dilution (ID) method. The remaining 2/3rd of the digested solution was used for the determination of the isotopic composition (IC) of Nd. The ID fractions of the samples were allowed to dry at about 90° C for equilibration of the spiked isotope thoroughly. The IC fractions were also dried to get the digested residue of the sample. The dried IC and ID fractions were dissolved in 2 ml of 2N HCl and were passed through Bio-Rad AG50-WX8 cation-exchange resin filled HCl columns. The bulk REE were eluted with 6N HCl after

ACCEPTED MANUSCRIPT

removing other cations using 2N HCl. The REE thus collected were dried and dissolved in 0.18 N HCl from which Sm and Nd were separated using HDEHP coated Teflon® resin with 0.4N and 0.3N HCl respectively. Before loading the REE, the HDEHP columns were equilibrated using 0.18 N calibrated HCl. Detailed procedure for sample digestion and chemical separation of Sm and Nd for isotope studies is given in Anand and Balakrishnan, (2010).

Nd and Sm were dissolved in 1 µl of 1N HNO_3 and were loaded on degassed and pre warmed 'Re' double filaments, and the analysis were carried out using the Thermal Ionization Mass Spectrometer (Triton – Thermo Finnigan) at Pondicherry University (data in Table 3). Procedural blanks were below 0.2 ng for Sm, and below 0.4 ng for Nd.

The isotopic composition of Nd was corrected for mass bias using the internal normalizing ratios of $^{146}Nd/^{144}Nd = 0.7219$. Mass fractionation correction for the spiked fraction was carried out by applying the external correction factors determined by multiple measurements of isotopic standard AMES for Nd. Reproducibility of the AMES standard was $^{143}Nd/^{144}Nd = 0.511971 \pm 9.8$ (2σ, n = 33) (recommended $^{143}Nd/^{144}Nd = 0.511968 \pm 4$; Govindaraju, 1994). The error of the $^{147}Sm/^{144}Nd$ is estimated to be better than 0.5%

The decay constant $\lambda^{147}Sm$ used is $6.54 \times 10^{-12} a^{-1}$. The εNd and Nd depleted mantle model ages (Nd T_{DM}) are calculated using the parameters $(^{143}Nd/^{144}Nd)_{CHUR} = 0.512638$, $(^{147}Sm/^{144}Nd)_{CHUR} = 0.1967$, $(^{143}Nd/^{144}Nd)_{DM} = 0.513151$ and $(^{147}Sm/^{144}Nd)_{DM} = 0.2136$.

References

Anand, R., Balakrishnan, S., 2010. Pb, Sr and Nd isotope systematics of metavolcanic rocks of the Hutti greenstone belt, Eastern Dharwar craton: Constraints on age, duration of volcanism and evolution of mantle sources during Late Archean. J. Asian Earth Sci. 39, 1–11.

Govindaraju, K., 1994. Compilation of working values and sample description for 383 geostandards. Geostandard. Newslett. 18, 1–158.

Stacey, J.S., Kramers, J.D., 1975. Approximation of terrestrial lead isotope evolution by a two stage model. Earth Planet. Sci. Lett. 26, 207–221.

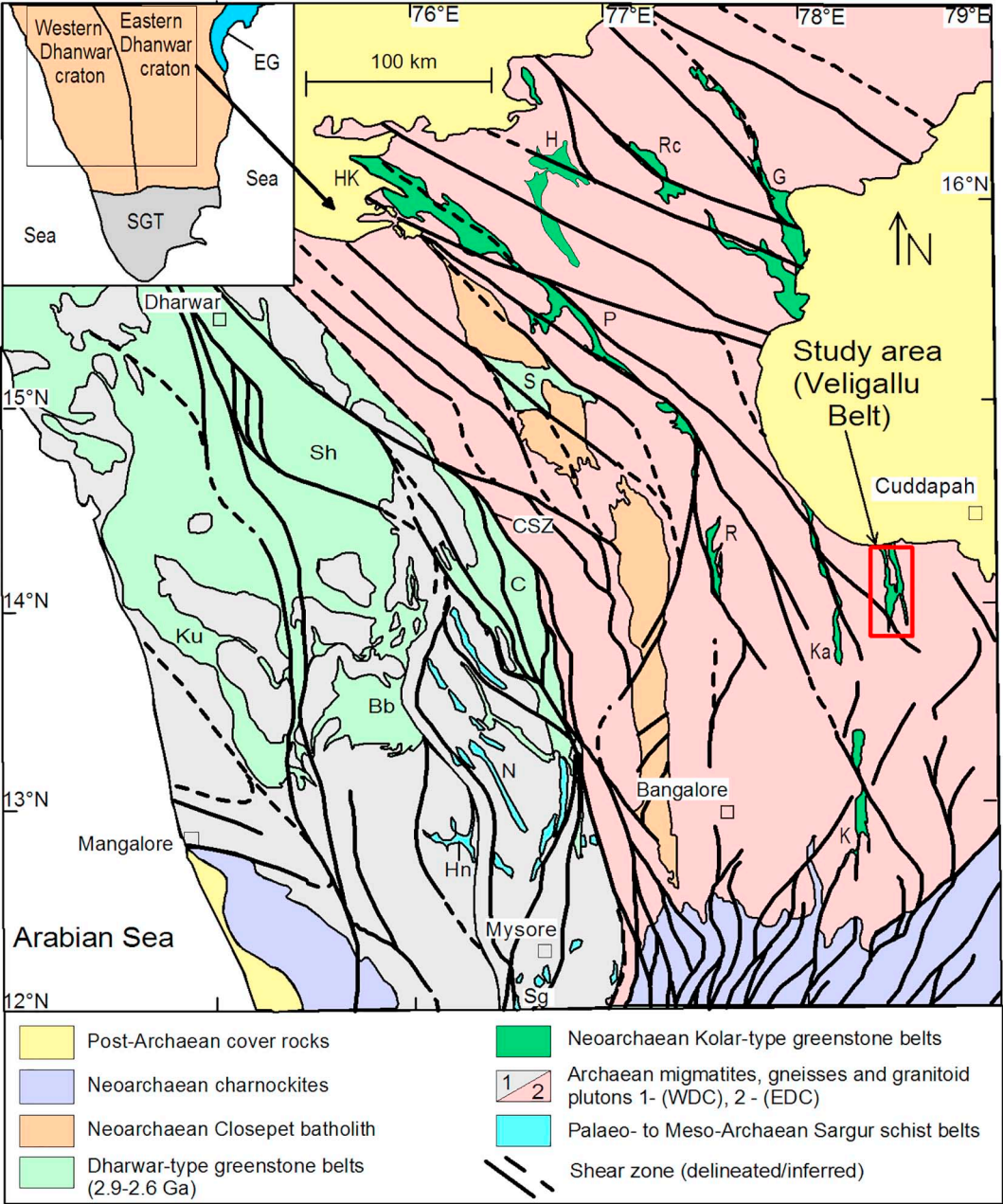
ACCEPTED MANUSCRIPT

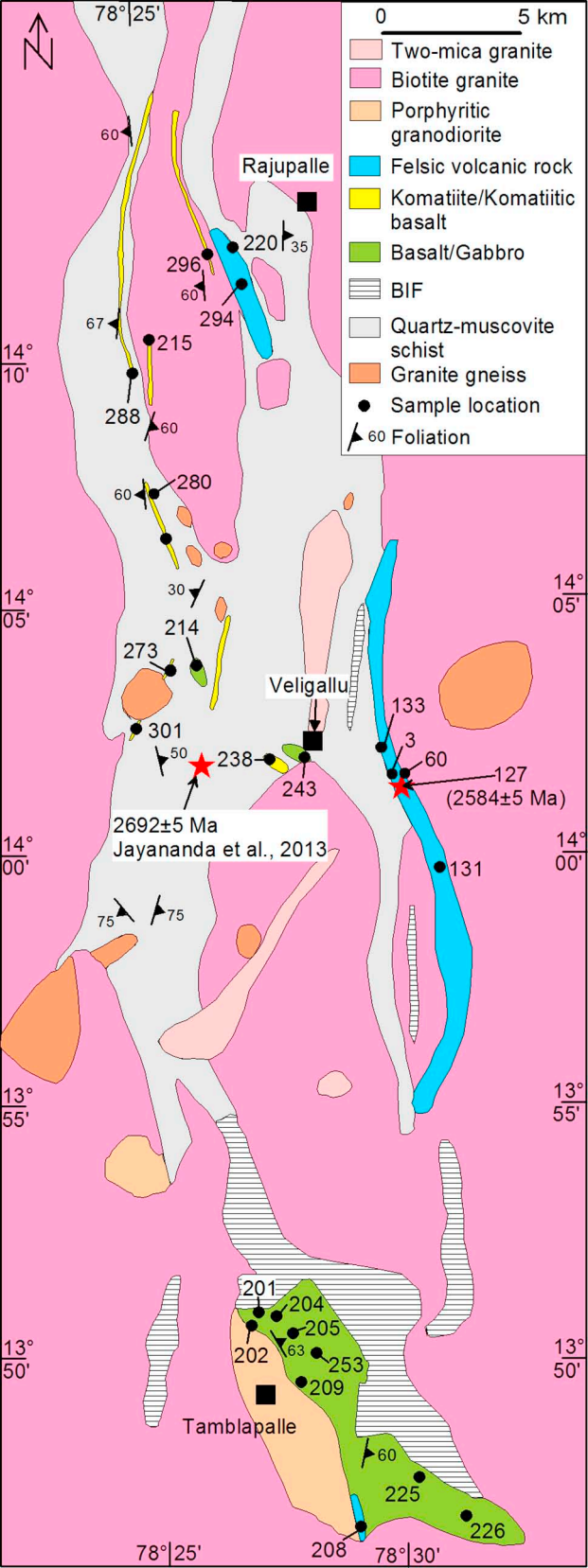
Whitehouse M.J., Kamber B.S., 2005. Assigning dates to thin gneissic veins in high-grade metamorphic terranes: A cautionary tale from Akilia, southwest Greenland. J. Petrol. 46, 291– 318.

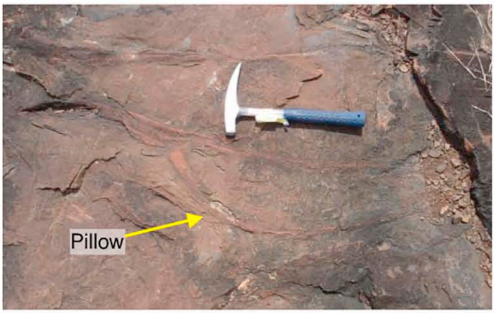
Whitehouse, M.J., Kamber, B.S., Moorbath, S., 1999. Age significance of U-Th-Pb zircon data from early Archaean rocks of West Greenland; a reassessment based on combined ion-microprobe and imaging studies. Chem. Geol. 160, 201–224.

Wiedenbeck, M., Allé, P., Corfu, F., Griffin, W.L., Meier, M., Oberli, F., Von Quadt, A., Roddick, J.C., Spiegel, W., 1995. Three natural zircon standards for U-Th-Pb, Lu-Hf, trace element and REE analyses. Geostandard. Newslett. 19, 1–23.

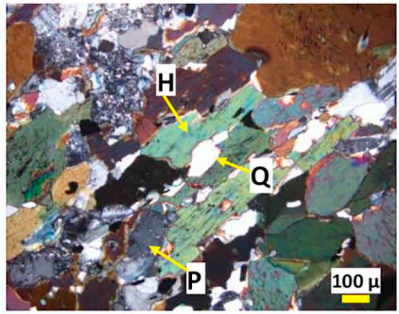
ACCEPTED MANUSCRIPT


Western Dhanwar craton
Eastern Dhanwar craton
EG
Sea
SGT
Sea
76°E
77°E
78°E
79°E
100 km
HK
H
Rc
G
16°N
N
Dharwar
P
Study area (Veligallu Belt)
15°N
S
Sh
Cuddapah
CSZ
R
C
14°N
Ku
Ka
Bb
N
Bangalore
13°N
Mangalore
K
Hn
Arabian Sea
Mysore
12°N
Sg
Post-Archaean cover rocks
Neoarchaean charnockites
Neoarchaean Closepet batholith
Dharwar-type greenstone belts (2.9-2.6 Ga)
Neoarchaean Kolar-type greenstone belts
1
2
Archaean migmatites, gneisses and granitoid plutons 1- (WDC), 2 - (EDC)
Palaeo- to Meso-Archaean Sargur schist belts
Shear zone (delineated/inferred)


78°25'
0
5 km
Two-mica granite
Biotite granite
Porphyritic granodiorite
Felsic volcanic rock
Komatiite/Komatiitic basalt
Basalt/Gabbro
BIF
Quartz-muscovite schist
Granite gneiss
Sample location
60 Foliation
Rajupalle
Veligallu
Tamblapalle
14° 10'
14° 05'
14° 00'
13° 55'
13° 50'
78°30'
60
220
35
296
60
294
67
215
288
60
280
60
30
214
273
301
50
238
243
133
3
60
127
(2584±5 Ma)
131
2692±5 Ma
Jayananda et al., 2013
75
75
201
204
205
202
63
253
209
60
225
226
208


Pillow

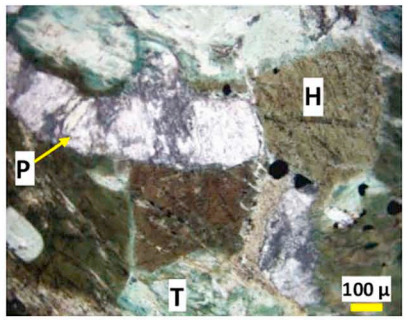
a


H
Q
P
100 µ

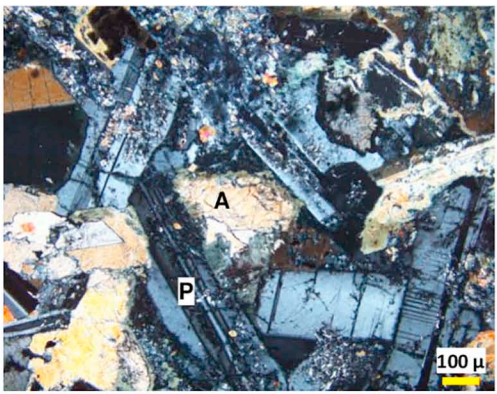
b



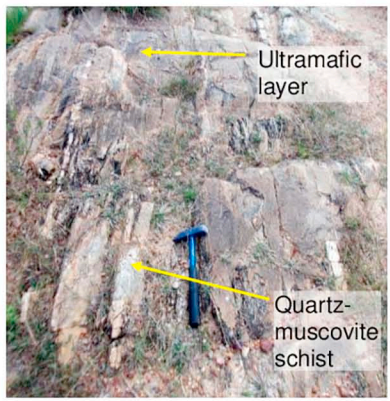
c


H
P
T
100 µ

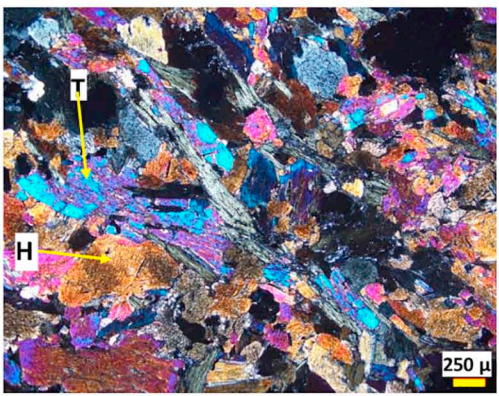
d


A
P
100 µ

e


Ultramafic layer
Quartz-muscovite schist

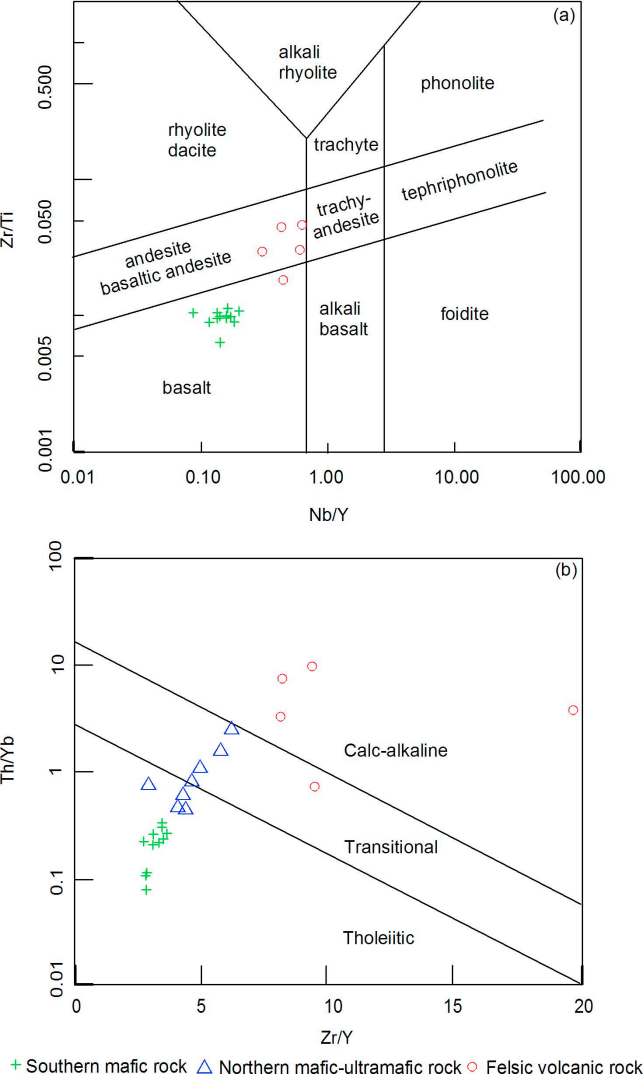
f

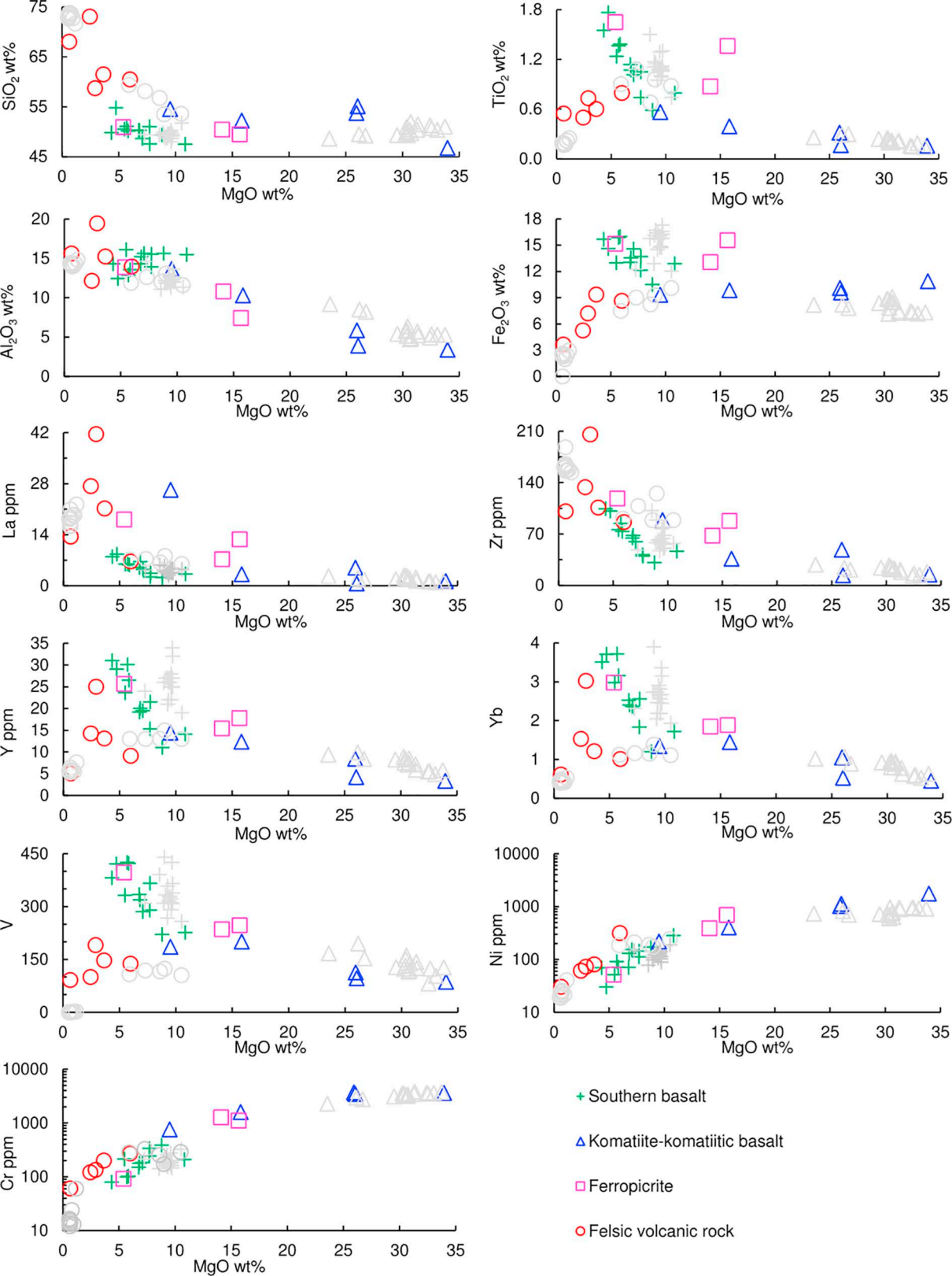

T
H
250 µ

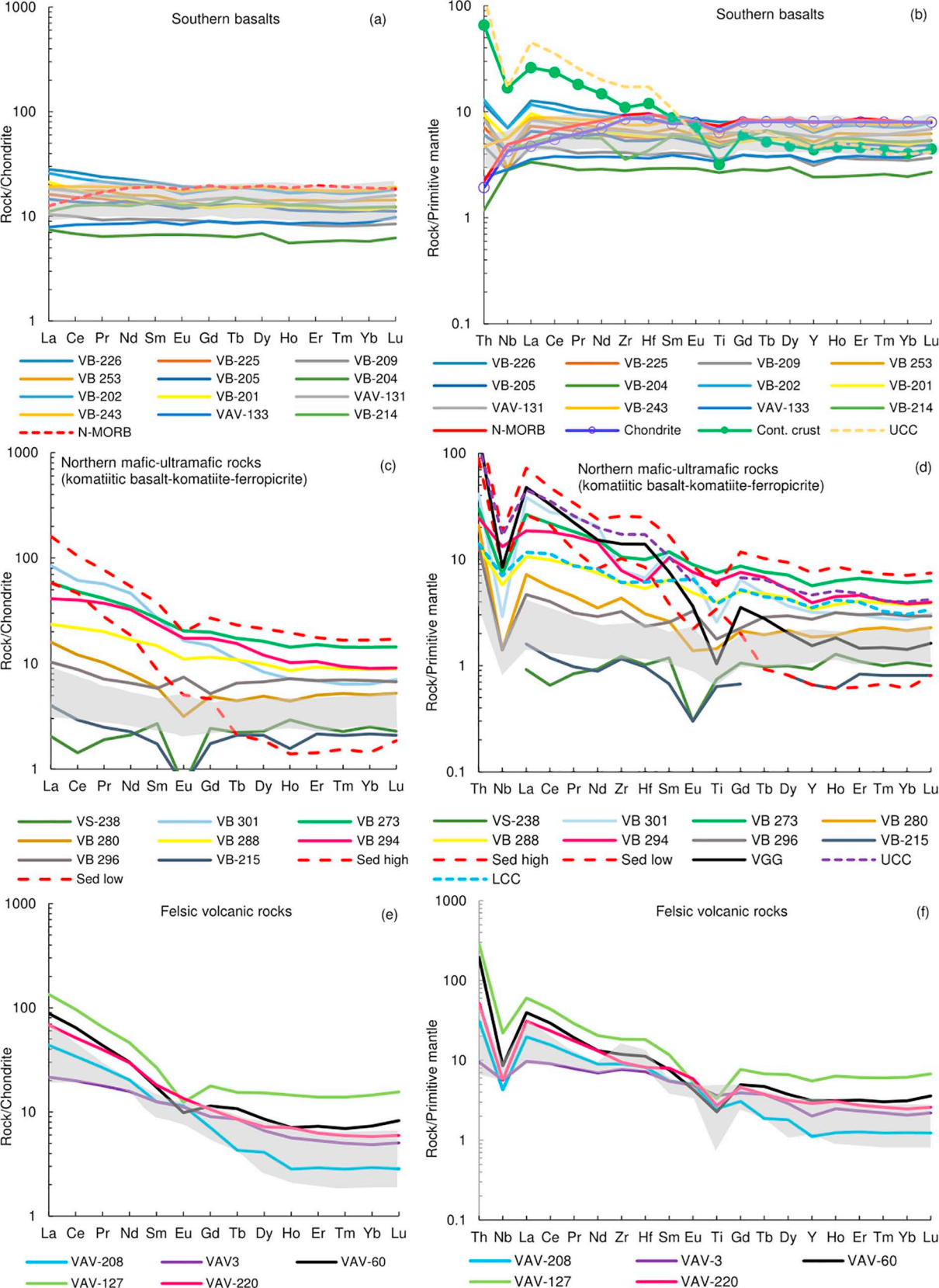
g

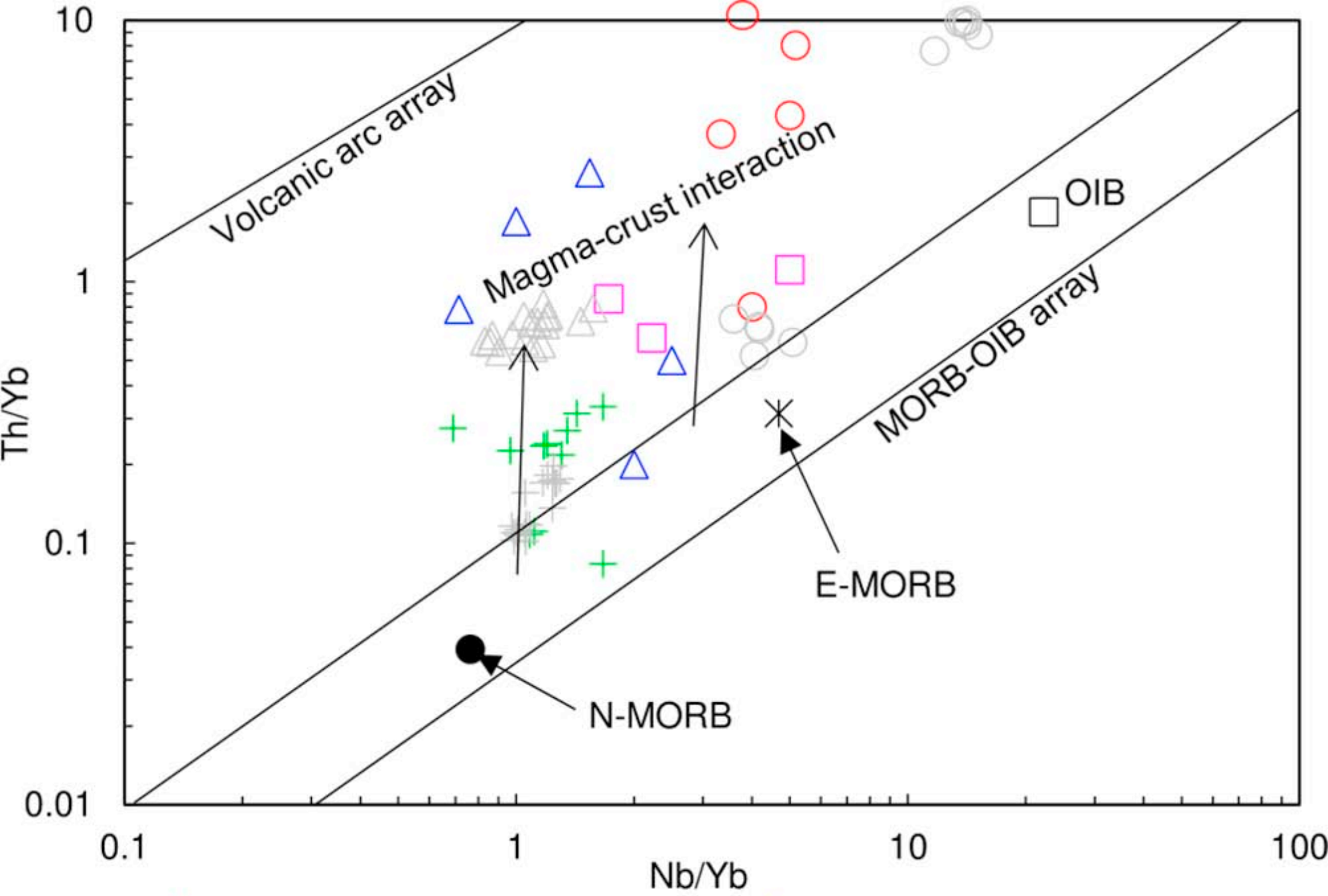


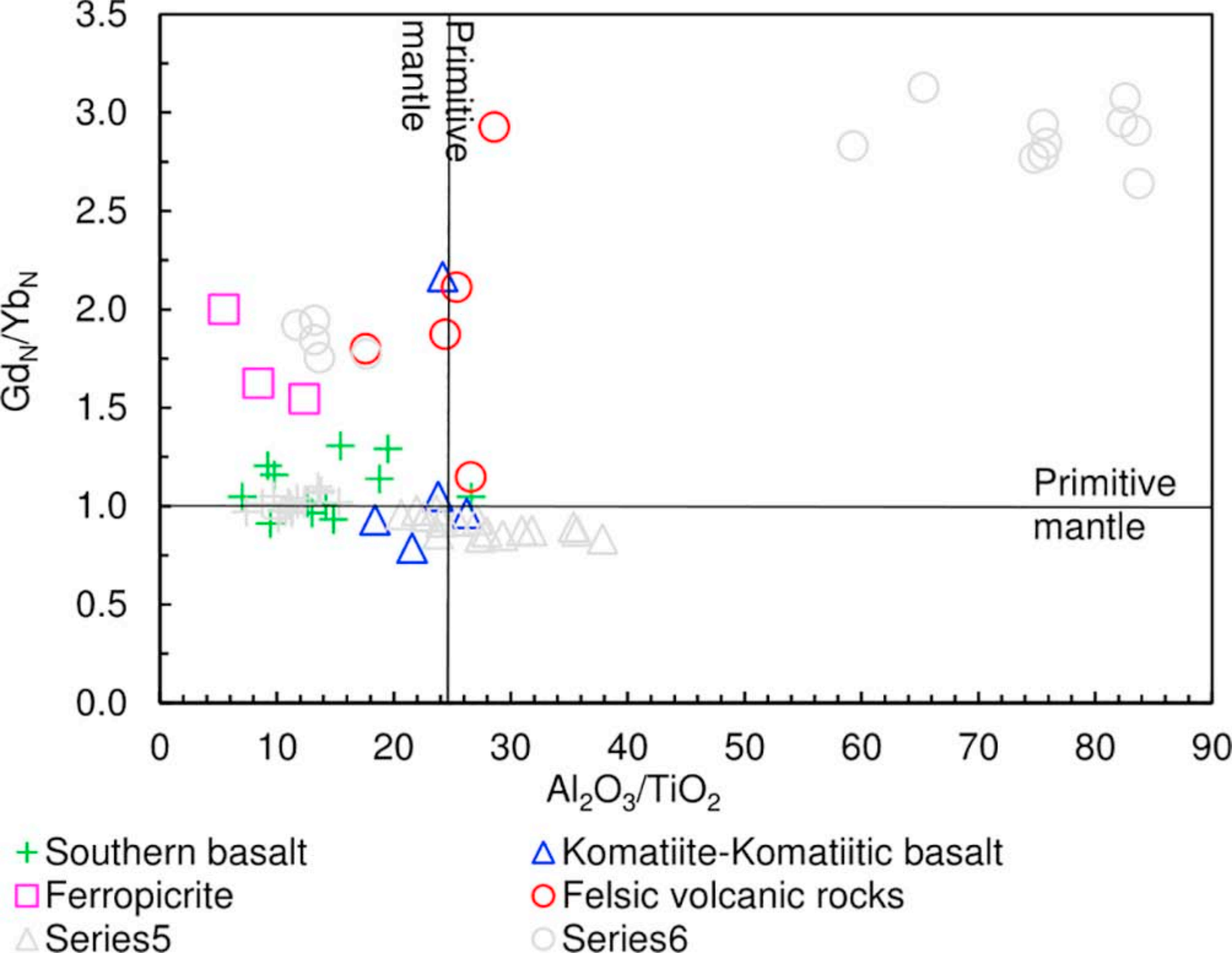
h


(a)
alkali rhyolite
phonolite
rhyolite dacite
trachyte
tephriphonolite
trachy-andesite
andesite basaltic andesite
alkali basalt
foidite
basalt
Zr/Ti
0.500
0.050
0.005
0.001
0.01
0.10
1.00
10.00
100.00
Nb/Y
(b)
Calc-alkaline
Transitional
Tholeiitic
Th/Yb
100
10
1
0.1
0.01
0
5
10
15
20
Zr/Y
Southern mafic rock
Northern mafic-ultramafic rock
Felsic volcanic rock


SiO2 wt%
MgO wt%
TiO2 wt%
Al2O3 wt%
Fe2O3 wt%
La ppm
Zr ppm
Y ppm
Yb
V
Ni ppm
Cr ppm
Southern basalt
Komatiite-komatiitic basalt
Ferropicrite
Felsic volcanic rock

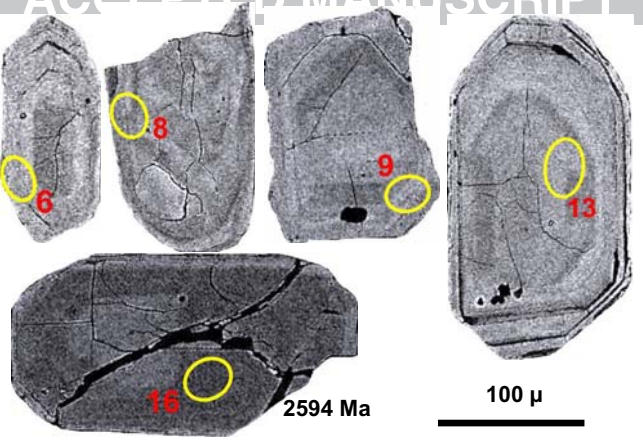

Southern basalts
(a)
Rock/Chondrite
1000
100
10
1
La Ce Pr Nd Sm Eu Gd Tb Dy Ho Er Tm Yb Lu
VB-226
VB-225
VB-209
VB 253
VB-205
VB-204
VB-202
VB-201
VAV-131
VB-243
VAV-133
VB-214
N-MORB
Southern basalts
(b)
Rock/Primitive mantle
100
10
1
0.1
Th Nb La Ce Pr Nd Zr Hf Sm Eu Ti Gd Tb Dy Y Ho Er Tm Yb Lu
VB-226
VB-225
VB-209
VB 253
VB-205
VB-204
VB-202
VB-201
VAV-131
VB-243
VAV-133
VB-214
N-MORB
Chondrite
Cont. crust
UCC
Northern mafic-ultramafic rocks
(komatiitic basalt-komatiite-ferropicrite)
(c)
Rock/Chondrite
1000
100
10
1
La Ce Pr Nd Sm Eu Gd Tb Dy Ho Er Tm Yb Lu
VS-238
VB 301
VB 273
VB 280
VB 288
VB 294
VB 296
VB-215
Sed high
Sed low
Northern mafic-ultramafic rocks
(komatiitic basalt-komatiite-ferropicrite)
(d)
Rock/Primitive mantle
100
10
1
0.1
Th Nb La Ce Pr Nd Zr Hf Sm Eu Ti Gd Tb Dy Y Ho Er Tm Yb Lu
VS-238
VB 301
VB 273
VB 280
VB 288
VB 294
VB 296
VB-215
Sed high
Sed low
VGG
UCC
LCC
Felsic volcanic rocks
(e)
Rock/Chondrite
1000
100
10
1
La Ce Pr Nd Sm Eu Gd Tb Dy Ho Er Tm Yb Lu
VAV-208
VAV3
VAV-60
VAV-127
VAV-220
Felsic volcanic rocks
(f)
Rock/Primitive mantle
1000
100
10
1
0.1
Th Nb La Ce Pr Nd Zr Hf Sm Eu Ti Gd Tb Dy Y Ho Er Tm Yb Lu
VAV-208
VAV-3
VAV-60
VAV-127
VAV-220


10
1
0.1
0.01
Th/Yb
0.1
1
10
100
Nb/Yb
Volcanic arc array
Magma-crust interaction
OIB
MORB-OIB array
E-MORB
N-MORB
Southern basalt
Komatiite-Komatiitic basalt
Ferropicrite
Felsic volcanic rock

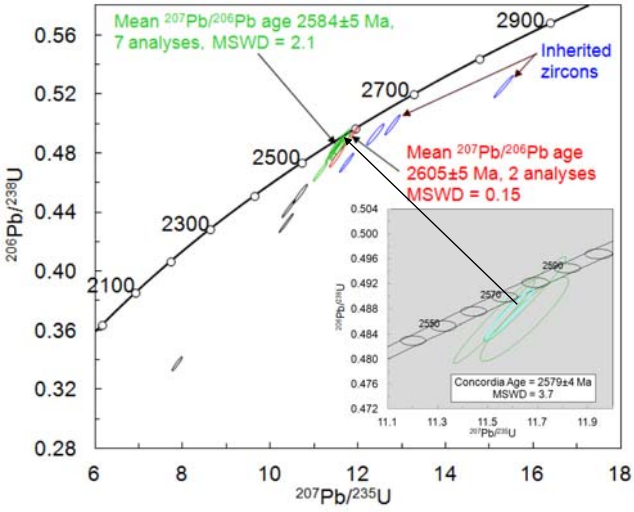

3.5
3.0
2.5
2.0
1.5
1.0
0.5
0.0
Gd_N/Yb_N
0
10
20
30
40
50
60
70
80
90
Al_2O_3/TiO_2
Primitive mantle
Primitive mantle
Southern basalt
Komatiite-Komatiitic basalt
Ferropicrite
Felsic volcanic rocks
Series5
Series6

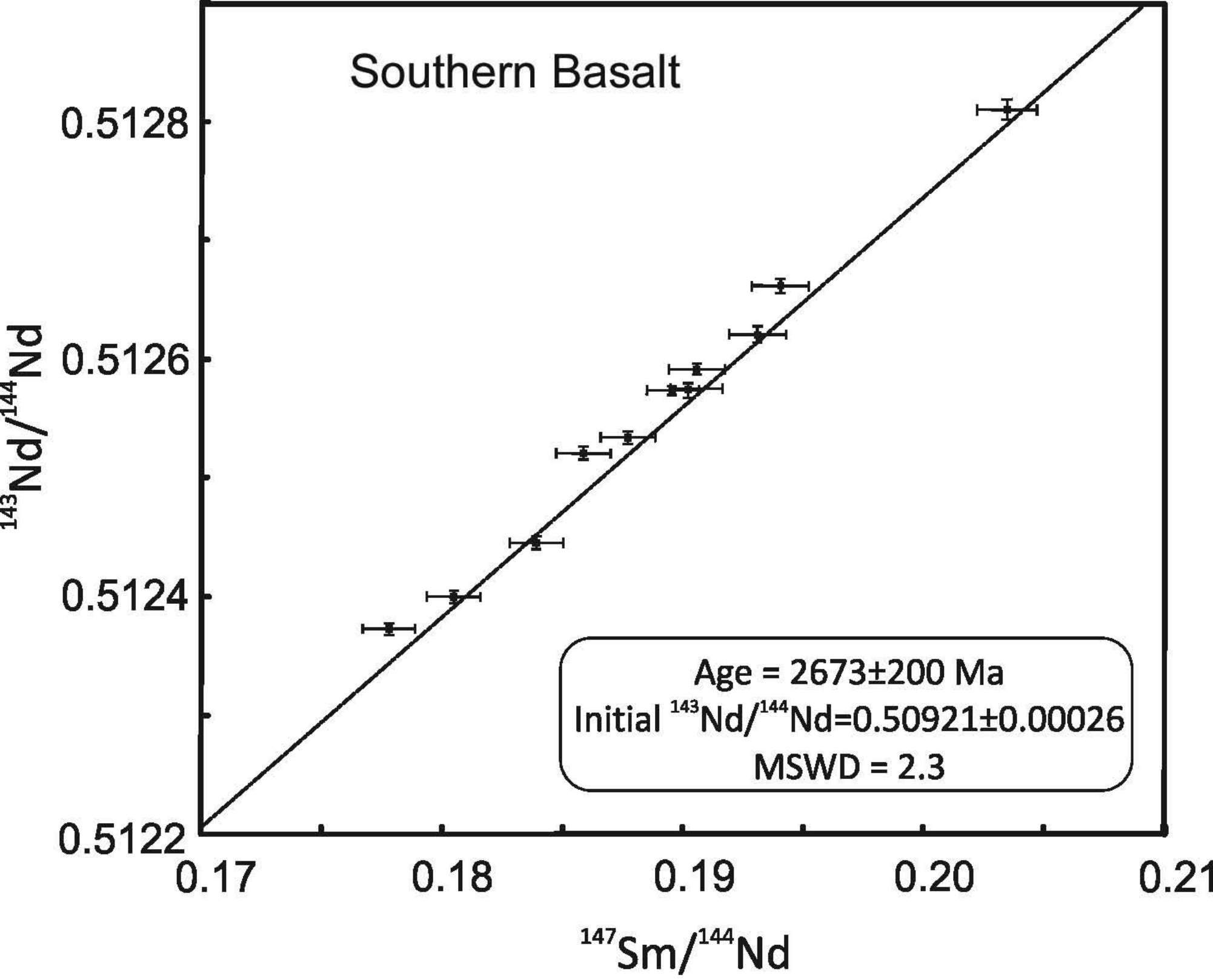
a

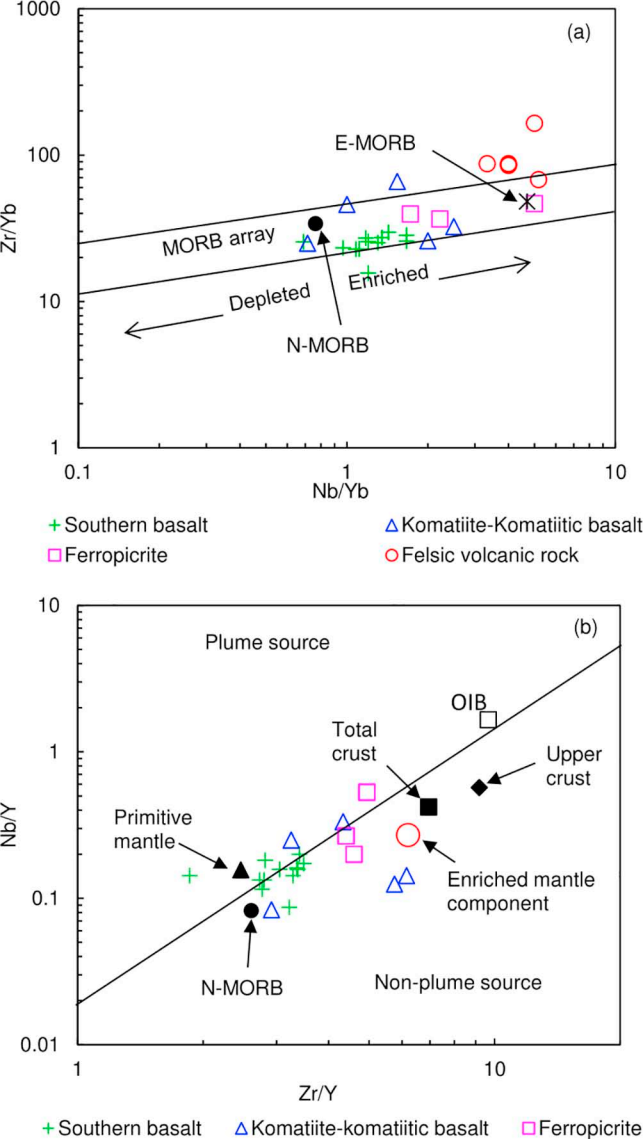
ACCEPTED MANUSCRIPT

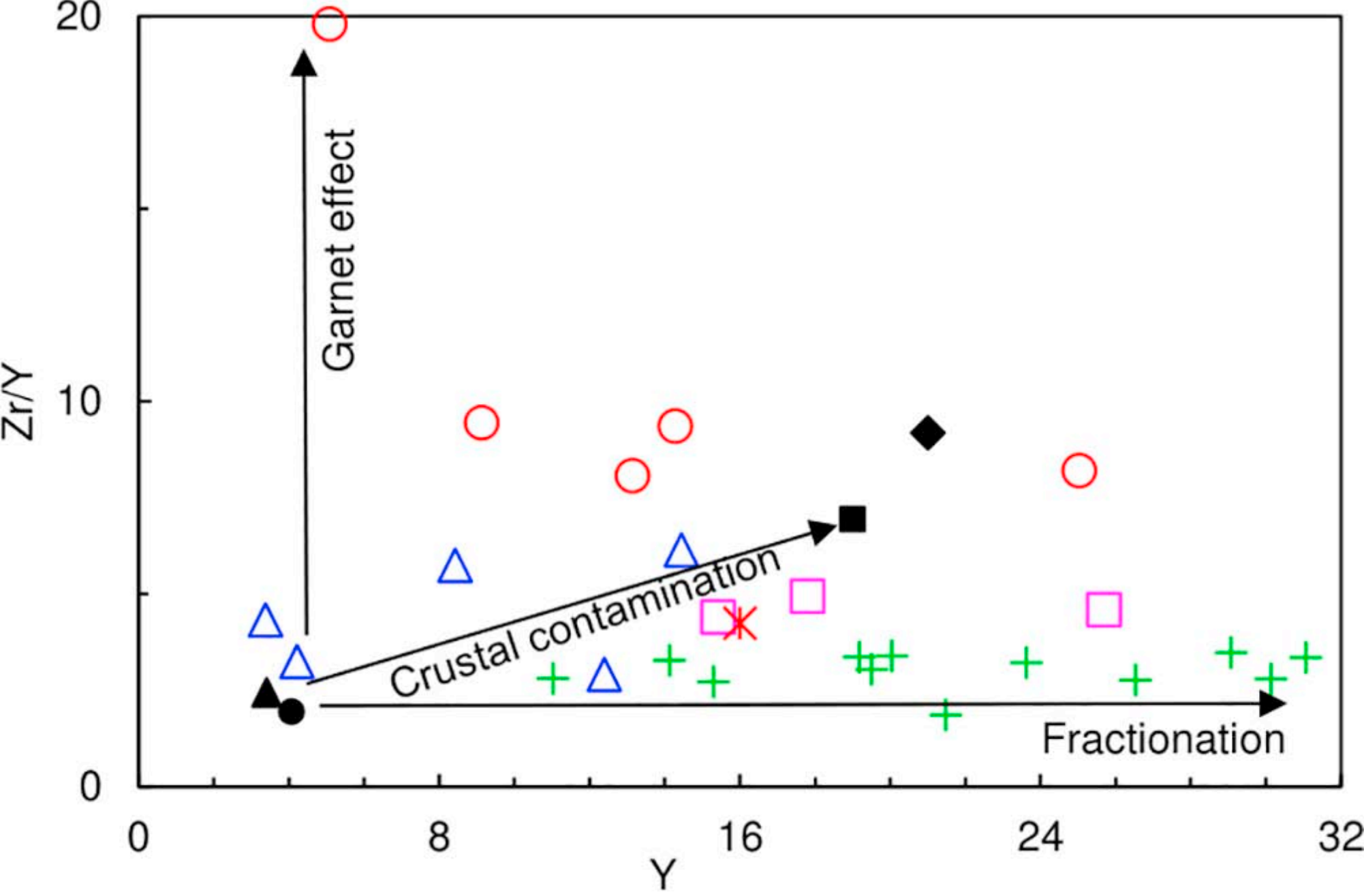


b




Southern Basalt
0.5128
0.5126
0.5124
0.5122
$^{143}Nd/^{144}Nd$
0.17
0.18
0.19
0.20
0.21
$^{147}Sm/^{144}Nd$
Age = 2673±200 Ma
Initial $^{143}Nd/^{144}Nd$=0.50921±0.00026
MSWD = 2.3


(a)
1000
100
10
1
Zr/Yb
0.1
1
10
Nb/Yb
E-MORB
MORB array
Depleted
Enriched
N-MORB
Southern basalt
Komatiite-Komatiitic basalt
Ferropicrite
Felsic volcanic rock
(b)
10
1
0.1
0.01
Nb/Y
1
10
Zr/Y
Plume source
OIB
Total crust
Upper crust
Primitive mantle
Enriched mantle component
N-MORB
Non-plume source
Southern basalt
Komatiite-komatiitic basalt
Ferropicrite


20
10
0
Zr/Y
Garnet effect
Crustal contamination
Fractionation
0
8
16
24
32
Y
Southern basalt
Komatiite-komatiitic basalt
Ferropicrite
Felsic volcanic rock
Upper continental crust
Lower continental crust
Total continental crust
Depleted mantle
Primitive mantle

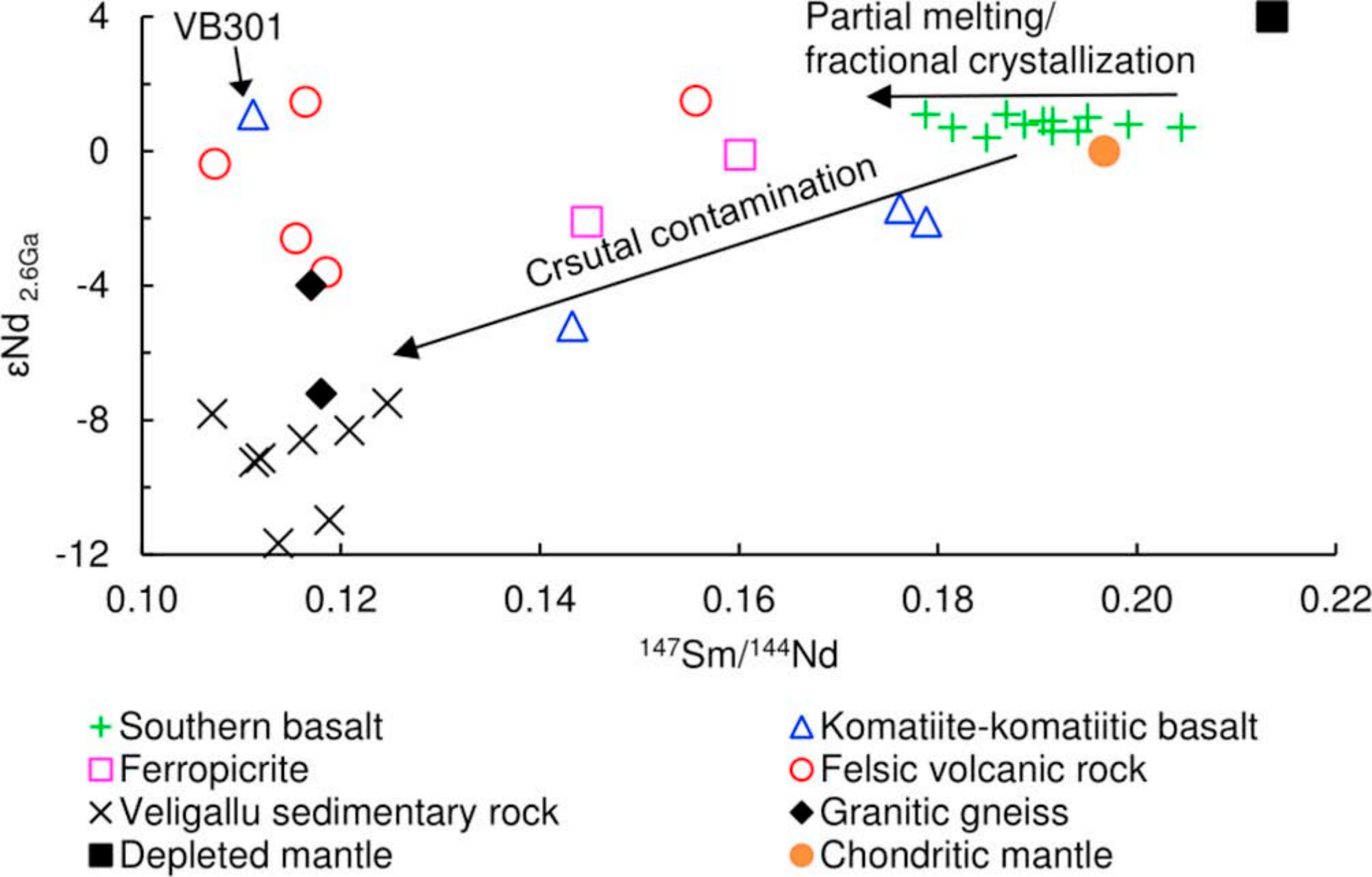

VB301
Partial melting/
fractional crystallization
Crsutal contamination
4
0
-4
-8
-12
εNd 2.6Ga
0.10
0.12
0.14
0.16
0.18
0.20
0.22
147Sm/144Nd
Southern basalt
Komatiite-komatiitic basalt
Ferropicrite
Felsic volcanic rock
Veligallu sedimentary rock
Granitic gneiss
Depleted mantle
Chondritic mantle

Table 1 Major (wt%) and trace (ppm) element compositions of metaigneous rocks from the Veligallu greenstone belt, eastern Dharwar craton, India

Serial No.	1	2	3	4	5	6	7	8	9
Rock type	Southern tholeiitic basalts								
Sample No.	VB226	VB225	VB209	VB253	VB205	VB204	VB202	VB201	VAV131
SiO_2	54.69	49.79	47.07	49.22	47.37	49.26	49.73	50.17	49.17
TiO_2	1.762	1.126	0.787	1.207	0.988	0.586	1.548	1.070	1.357
Al_2O_3	12.41	14.19	15.34	15.70	15.24	15.61	14.29	15.18	13.29
Fe_2O_3(T)	14.58	12.90	12.76	12.63	14.19	10.48	15.64	13.52	15.67
MnO	0.234	0.190	0.190	0.179	0.176	0.159	0.194	0.187	0.215
MgO	4.73	6.70	10.74	5.35	6.88	8.77	4.33	6.81	5.72
CaO	8.38	11.36	10.39	9.24	9.30	13.14	12.22	10.76	9.80
Na_2O	2.64	2.53	1.29	3.63	2.76	1.65	1.54	1.87	1.95
K_2O	0.18	0.19	0.46	0.13	0.42	0.05	0.18	0.15	0.72
P_2O_5	0.15	0.08	0.07	0.10	0.10	0.04	0.14	0.09	0.12
LOI	0.29	0.79	1.70	0.63	1.30	0.83	0.41	0.98	1.74
Total	100.046	99.85	100.80	98.02	98.72	100.58	100.22	100.79	99.75
Mg#	0.39	0.51	0.63	0.46	0.49	0.62	0.35	0.50	0.42
Sc	43	50	30	43	35	37	40	41	41
V	420	331	224	323	278	220	381	318	414
Ba	33	25	15	53	78	19	31	31	76
Sr	92	125	87	133	110	133	172	118	124
Y	29	19	14	23	19	11	31	20	26
Zr	101	64	46	74	58	31	104	68	72
Cr	< 20	150	210	210	180	390	80	180	100
Ni	30	70	280	50	150	170	70	130	70
Cu	< 10	140	80	120	150	100	120	130	240
Zn	170	110	90	60	180	70	130	110	130
Ga	18	17	15	18	18	14	19	17	17
Rb	14	6	72	2	12	< 2	3	3	39
Nb	5	3	2	2	3	2	5	4	3
Cs	< 0.5	0.6	9.4	< 0.5	1.3	< 0.5	< 0.5	< 0.5	6.0
La	8.7	5.0	3.2	5.8	4.4	2.3	8.0	6.6	5.6
Ce	21.2	12.2	8.0	13.7	10.8	5.5	18.7	14.5	13.7
Pr	2.91	1.79	1.11	2.09	1.57	0.78	2.61	1.89	1.89
Nd	13.5	8.0	5.6	9.3	8.2	3.9	12.0	8.8	9.0
Sm	4.1	2.7	1.8	3.0	2.5	1.3	3.8	2.6	2.6
Eu	1.41	0.99	0.67	0.99	0.85	0.49	1.20	0.98	1.01
Gd	4.8	3.3	2.3	3.7	3.2	1.7	4.6	3.1	3.7
Tb	0.9	0.6	0.4	0.7	0.6	0.3	0.9	0.6	0.7
Dy	5.9	4.1	2.8	4.4	3.9	2.2	5.8	4.0	4.5
Ho	1.2	0.9	0.6	1.0	0.8	0.4	1.2	0.9	0.9
Er	3.6	2.5	1.7	2.9	2.3	1.2	3.6	2.5	2.8
Tm	0.56	0.37	0.26	0.44	0.35	0.19	0.53	0.38	0.44
Yb	3.7	2.5	1.7	2.9	2.3	1.2	3.5	2.4	3.1
Lu	0.6	0.39	0.27	0.45	0.35	0.20	0.58	0.40	0.50
Hf	2.8	1.7	1.2	1.9	1.6	0.9	2.5	1.8	1.9
Ta	1	0.5	0.3	0.3	0.5	0.3	0.6	0.5	0.6
Pb	< 5	< 5	< 5	< 5	< 5	< 5	< 5	< 5	< 5
Th	1.0	0.6	0.4	0.8	0.5	0.1	1.1	0.8	0.7
U	0.3	0.2	0.2	0.2	0.2	< 0.1	0.4	0.3	0.2
Ti/Nb	2111	2248	2357	3615	1973	1755	1855	1602	2709
Zr/Nb	20	21	23	37	19	16	21	17	24
$(La/Sm)_{PM}$	1.4	1.2	1.1	1.2	1.1	1.1	1.4	1.6	1.4
Th/Ce	0.05	0.05	0.05	0.06	0.05	0.02	0.06	0.06	0.05
Nb/Th	5.0	5.0	5.0	2.5	6.0	20.0	4.5	5.0	4.3
La/Nb	1.7	1.7	1.6	2.9	1.5	1.2	1.6	1.7	1.9
Lattitude	13°46'53"N	13°47'40"N	13°49'32"N	13°50'31"N	13°50'51"N	13°50'53"N	13°50'40"N	13°50'55"N	13°59'21"N
Longitude	78°30'55"E	78°29'58"E	78°27'34"E	78°27'24"E	78°27'05"E	78°26'54"E	78°26'30"E	78°26'45"E	78°30'47"E

Major elements, Ba, Sr, Y, Zr, Be, Sc and V analyzed by fusion ICP-AES and other elements by fusion ICP-MS.
Details of analytical techniques are given in Appendix 1. Mg# = mol MgO/(MgO + FeO_{total}),

Table 1. Continued

Serial No.	10	11	12	13	14	15	16	17
Rock type	Southern tholeiitic basalts			Northern komatiites and komatiitic basalts				
Sample No.	VB243	VAV133	VB214	VS238	VB301	VB 280	VB 296	VB215
SiO_2	50.86	50.03	46.50	52.37	52.89	50.99	50.57	41.46
TiO_2	1.359	0.727	1.025	0.156	0.548	0.302	0.380	0.140
Al_2O_3	12.84	13.66	15.19	3.71	13.24	5.56	9.97	3.02
$Fe_2O_3(T)$	15.80	11.89	13.39	9.10	9.03	9.58	9.52	9.65
MnO	0.212	0.188	0.187	0.123	0.149	0.109	0.221	0.165
MgO	5.67	7.55	7.55	24.75	9.22	24.61	15.33	30.12
CaO	10.04	11.53	11.44	4.79	8.19	3.58	8.28	4.12
Na_2O	2.21	1.83	1.61	0.05	3.12	0.12	0.30	0.01
K_2O	0.43	0.57	0.77	< 0.01	0.37	0.02	2.21	< 0.01
P_2O_5	0.12	0.05	0.09	0.02	0.17	0.04	0.05	0.02
LOI	0.86	1.44	2.19	4.83	2.05	5.63	3.32	11.34
Total	100.40	99.47	99.94	99.90	98.99	100.50	100.20	100.00
Mg#	0.42	0.56	0.53	0.84	0.67	0.84	0.76	0.86
Sc	40	41	38	17	24	17	31	14
V	423	284	358	92	180	107	194	77
Ba	52	86	104	9	135	9	292	50
Sr	101	94	115	3	355	6	43	23
Y	30	15	21	4	14	8	12	3
Zr	84	41	39	13	86	46	35	13
Cr	100	240	330	3330	740	3530	1560	3220
Ni	90	110	140	1070	210	970	390	1560
Cu	120	90	190	90	20	< 10	< 10	20
Zn	130	100	110	120	80	100	90	60
Ga	17	14	16	4	16	7	10	3
Rb	7	12	25	< 2	8	< 2	96	< 2
Nb	4	2	3	1	2	1	1	1
Cs	< 0.5	0.7	< 0.5	< 0.5	< 0.5	< 0.5	12.6	< 0.5
La	6.0	2.4	3.4	0.6	25.5	4.7	3.1	1.1
Ce	15.5	6.6	10.0	1.1	48.1	9.3	6.9	2.1
Pr	2.32	1.01	1.54	0.22	6.72	1.18	0.84	0.27
Nd	11.3	5.0	7.4	1.2	27.0	4.5	3.8	1.2
Sm	3.7	1.7	2.6	0.5	5.1	1.1	1.1	0.3
Eu	1.27	0.60	0.91	< 0.05	1.18	0.22	0.53	< 0.05
Gd	4.7	2.3	3.3	0.6	3.7	1.2	1.3	0.4
Tb	0.9	0.4	0.7	0.1	0.5	0.2	0.3	< 0.1
Dy	6.1	2.8	4.3	0.7	2.6	1.5	2.1	0.6
Ho	1.3	0.6	0.9	0.2	0.5	0.3	0.5	0.1
Er	3.7	1.8	2.6	0.5	1.4	1.0	1.4	0.4
Tm	0.56	0.27	0.38	0.07	0.20	0.16	0.22	0.06
Yb	3.7	1.8	2.5	0.5	1.3	1.0	1.4	0.4
Lu	0.61	0.31	0.39	0.07	0.22	0.16	0.21	0.06
Hf	2.3	1.1	1.3	0.3	2.0	0.9	0.7	0.3
Ta	0.9	0.8	0.3	< 0.1	0.1	< 0.1	< 0.1	< 0.1
Pb	< 5	< 5	17	< 5	7	< 5	< 5	< 5
Th	0.4	0.2	< 0.1	0.1	3.4	1.7	1.1	0.2
U	0.2	0.1	< 0.1	< 0.1	0.9	0.3	0.5	< 0.1
Ti/Nb	2035	2177	2047	934	1641	1809	2276	839
Zr/Nb	21	21	13	13	43	46	35	13
$(La/Sm)_{PM}$	1.0	0.9	0.8	0.8	3.2	2.8	1.8	2.4
Th/Ce	0.03	0.03	<0.01	0.09	0.07	0.18	0.16	0.10
Nb/Th	10.0	10.0	>30	10.0	0.6	0.6	0.9	5.0
La/Nb	1.5	1.2	1.1	0.6	12.8	4.7	3.1	1.1
Latitude	14°01'52"N	14°01'58"N	14°03'50"N	14°01'51"N	14°02'29"N	14°07'16"N	14°11'50"N	14°10'12"N
Longitude	78°27'39"E	78°29'30"E	78°25'36"E	78°26'56"E	78°24'20"E	78°24'56"E	78°25'49"E	78°24'40"E

Table 1. Continued

Serial No.	18	19	20	21	22	23	24	25
Rock type	Ferropicrites			Felsic volcanic rocks				
Sample No.	VB 273	VB 288	VB 294	VAV208	VAV3	VAV60	VAV127	VAV220
SiO_2	49.57	49.05	47.25	66.90	59.68	71.61	56.30	60.87
TiO_2	1.605	0.851	1.301	0.538	0.784	0.489	0.702	0.595
Al_2O_3	13.50	10.52	7.08	15.38	13.79	11.93	18.65	15.09
$Fe_2O_3(T)$	14.74	12.71	14.86	3.58	8.52	5.13	6.91	9.26
MnO	0.211	0.190	0.257	0.035	0.126	0.074	0.102	0.234
MgO	5.25	13.71	14.95	0.63	5.90	2.39	2.78	3.61
CaO	9.01	8.62	9.16	4.50	6.32	1.48	2.62	4.43
Na_2O	1.88	1.42	0.45	4.40	2.90	2.62	7.64	3.52
K_2O	1.33	0.16	0.08	2.25	0.54	2.27	0.11	1.20
P_2O_5	0.21	0.08	0.09	0.12	0.11	0.06	0.06	0.16
LOI	1.66	3.16	3.21	0.44	1.13	1.95	2.51	1.70
Total	98.98	100.50	98.69	98.76	99.80	100.00	98.38	100.70
Mg#	0.41	0.68	0.67	0.26	0.58	0.48	0.44	0.44
Sc	40	31	29	9	17	14	19	18
V	386	229	236	90	136	98	183	146
Ba	401	49	7	543	148	1118	134	424
Sr	225	80	46	649	338	123	167	331
Y	25	15	17	5	9	14	24	13
Zr	115	66	84	99	85	131	197	105
Cr	90	1250	1070	60	270	120	130	200
Ni	50	380	660	30	310	60	70	80
Cu	80	90	130	20	70	80	40	40
Zn	120	100	180	70	90	60	120	80
Ga	20	13	12	19	19	13	21	17
Rb	34	2	< 2	84	36	73	2	35
Nb	5	4	9	3	4	6	15	4
Cs	1.2	< 0.5	< 0.5	7.6	1.9	1.0	< 0.5	3.6
La	17.7	7.1	12.2	13.3	6.6	26.8	39.9	21.0
Ce	37.8	17.1	30.9	27.2	15.9	51.0	74.7	41.2
Pr	4.91	2.38	4.36	3.19	2.15	5.20	7.62	4.79
Nd	20.1	9.8	18.6	11.9	9.3	17.6	26.6	17.6
Sm	5.1	2.8	4.4	2.4	2.4	3.3	5.0	3.5
Eu	1.46	0.79	1.22	0.83	0.81	0.71	0.87	0.98
Gd	5.0	2.9	4.3	1.8	2.3	2.9	4.4	2.7
Tb	0.8	0.5	0.7	0.2	0.4	0.5	0.7	0.4
Dy	5.1	3.1	3.7	1.3	2.1	2.7	4.7	2.3
Ho	1.0	0.6	0.7	0.2	0.4	0.5	1.0	0.5
Er	3.1	1.9	2.1	0.6	1.1	1.5	2.8	1.3
Tm	0.45	0.28	0.29	0.09	0.16	0.22	0.43	0.19
Yb	2.9	1.8	1.8	0.6	1.0	1.5	2.9	1.2
Lu	0.45	0.28	0.28	0.09	0.16	0.26	0.48	0.19
Hf	3.0	1.6	1.8	2.5	2.2	3.4	5.4	2.5
Ta	0.4	0.3	0.5	1.3	0.9	0.8	2.5	0.7
Pb	< 5	6	32	10	< 5	16	23	18
Th	2.5	1.1	2.0	2.6	0.8	16.2	23.3	4.4
U	0.5	0.2	0.7	0.8	0.2	3.5	10.7	1.4
Ti/Nb	1923	1274	866	1074	1174	488	280	891
Zr/Nb	23	16.5	9.3	33	21	22	13	26
$(La/Sm)_{PM}$	2.2	1.6	1.8	3.6	1.8	5.2	5.2	3.9
Th/Ce	0.07	0.06	0.06	0.10	0.05	0.32	0.31	0.11
Nb/Th	2.0	3.6	4.5	1.2	5.0	0.4	0.6	0.9
La/Nb	3.5	1.8	1.4	4.4	1.7	4.5	2.7	5.3
Latitude	14°03'50"N	14°09'08"N	14°11'28"N	13°46'41"N	14°01'17"N	14°01'19"N	14°01'06"N	14°12'10"N
Longitude	78°25'08"E	78°24'08"E	78°26'23"E	78°28'46"E	78°29'32"E	78°29'45"E	78°29'48"E	78°26'01"E

Table 2. SIMS U-Pb age data for zircons of the felsic volcanic sample VAV217 from Veligallu greenstone belt.

spot #	Derived age (Ma)						Corrected ratios						r	Disc.	Elemental data					
	$^{206}Pb/^{238}U$	± 1σ	$^{207}Pb/^{235}U$	± 1σ	$^{207}Pb/^{206}Pb$	± 1σ	$^{206}Pb/^{238}U$	± 1σ (%)	$^{207}Pb/^{235}U$	± 1σ (%)	$^{207}Pb/^{206}Pb$	± 1σ (%)		%	U (ppm)	Th (ppm)	Pb (ppm)	Th/U (meas.)	$^{206}Pb/^{204}Pb$ (meas.)	f_{206}%
n4429-01	2529.0	19.0	2559.0	8.7	2582.9	3.0	0.48039	0.90893	11.43158	0.93	0.172588	0.18	0.98	-2.5	399.6	267.6	261.2	0.67	194021	0.01
n4429-02	2406.4	18.9	2496.0	9.1	2569.7	4.1	0.45251	0.93996	10.68339	0.97	0.171229	0.25	0.97	-7.6	458.3	259.5	277.5	0.57	48222	0.04
n4429-03	2535.6	19.1	2567.7	8.9	2593.1	4.1	0.48192	0.90965	11.53795	0.94	0.173641	0.25	0.96	-2.7	261.4	130.3	165.4	0.50	278840	{0.01}
n4429-04	1874.2	15.0	2215.9	8.7	2548.8	4.7	0.33740	0.92333	7.86712	0.97	0.169109	0.28	0.96	-30.4	240.0	110.6	104.6	0.46	64230	0.03
n4429-05	2515.5	19.0	2566.2	8.8	2606.5	3.8	0.47731	0.90894	11.52004	0.94	0.175047	0.23	0.97	-4.2	258.2	162.4	166.4	0.63	48582	0.04
n4429-06	2316.1	19.7	2468.5	9.5	2596.5	2.6	0.43231	1.00978	10.37189	1.02	0.174004	0.16	0.99	-12.8	576.6	381.9	339.6	0.66	89389	0.02
n4429-07	2362.0	18.0	2472.9	8.6	2565.3	3.1	0.44255	0.90896	10.42082	0.93	0.170780	0.18	0.98	-9.5	549.6	304.9	325.8	0.55	153125	0.01
n4429-08	2720.1	20.4	2835.9	8.9	2919.2	2.7	0.52494	0.91592	15.32810	0.93	0.211777	0.17	0.98	-8.4	364.7	163.8	256.7	0.45	175815	0.01
n4429-09	2553.1	19.2	2566.7	8.8	2577.4	3.7	0.48594	0.91165	11.52575	0.94	0.172022	0.22	0.97	-1.1	346.7	164.2	219.8	0.47	176568	0.01
n4429-10	2608.7	19.5	2664.3	8.8	2706.8	3.6	0.49881	0.90930	12.78994	0.93	0.185965	0.22	0.97	-4.4	250.0	74.3	158.3	0.30	341113	{0.01}
n4429-11	2538.6	19.5	2562.4	8.8	2581.2	2.6	0.48261	0.92742	11.47280	0.94	0.172413	0.16	0.99	-2.0	539.1	384.1	356.6	0.71	72528	0.03
n4429-12	2580.9	20.2	2635.2	9.3	2677.2	4.6	0.49237	0.94662	12.40059	0.99	0.182664	0.28	0.96	-4.4	242.1	202.4	169.0	0.84	95255	0.02
n4429-13	2572.6	20.7	2590.6	9.3	2604.7	2.8	0.49044	0.97523	11.82451	0.99	0.174864	0.17	0.99	-1.5	456.6	171.2	286.5	0.37	182804	0.01
n4429-14	2498.9	18.9	2583.8	8.7	2651.0	3.1	0.47350	0.90994	11.73848	0.93	0.179800	0.19	0.98	-6.9	362.8	238.9	233.4	0.66	86333	0.02
n4429-15	2470.5	18.9	2535.3	8.8	2587.5	3.3	0.46703	0.91732	11.14411	0.94	0.173063	0.20	0.98	-5.4	530.1	409.5	344.5	0.77	153981	0.01
n4429-16	2554.7	19.2	2576.5	9.4	2593.6	6.9	0.48632	0.91042	11.64700	1.00	0.173696	0.41	0.91	-1.8	111.8	61.2	72.4	0.55	120562	{0.02}
n4429-17	2568.9	19.3	2576.5	8.8	2582.5	3.6	0.48958	0.90991	11.64728	0.94	0.172544	0.22	0.97	-0.6	264.8	116.7	167.9	0.44	140598	0.01

Note: f_{206} (%) is the percentage of common ^{206}Pb, estimated from the measured ^{204}Pb. Figures in parentheses indicate ^{204}Pb counts below detection limit, so no correction has been applied.
Corrected data use present day Stacey and Kramers (1975) model Pb.

Table 3.

Sm-Nd isotopic data of metaigneous rocks of the Veligallu greenstone belt, eastern Dharwar craton.

Sample No.	Sm (ppm)	Nd (ppm)	$^{147}Sm/^{144}Nd$	$^{143}Nd/^{144}Nd$	Error ($x10^{-6}$) (2σ)	tDM (Ga)	εNd *2.6 Ga*	εNd *2.67 Ga*	εNd *2.58 Ga*	Suite
VB201	2.636	8.914	0.1788	0.512373	4			1.0		Southern tholeiitic basalts
VB202	3.848	12.58	0.1849	0.512446	5			0.3		
VB204	1.376	4.267	0.1950	0.512661	5			1.0		
VB205	2.607	8.351	0.1887	0.512534	4			0.7		
VB225	2.629	8.298	0.1915	0.512575	5			0.6		
VB243	3.639	11.334	0.1941	0.512621	6			0.6		
VB209	1.820	5.745	0.1916	0.512591	4			0.8		
VB226	2.459	7.798	0.1906	0.512574	3			0.9		
VAV131	3.070	9.931	0.1869	0.512521	4			1.1		
VAV133	1.793	5.302	0.2045	0.512810	7			0.7		
VB253	3.143	10.471	0.1815	0.512400	5			0.6		
VB253 (Repeat)	3.140	10.510	0.1806	0.512401	4			0.9		
VB288	2.9	10.946	0.1601	0.512001	4		-0.1	0.2		Northern ultramafic-mafic rocks (komatiites, komatiitic basalts, ferropicrites)
VB296	1.185	4.065	0.1762	0.512203	6		-1.7	-1.5		
VB301	5.173	28.128	0.1112	0.511226	4		1.1	1.8		
VB215	0.381	1.287	0.1788	0.512223	6		-2.1	-2.0		
VB215 (Repeat)	0.384	1.249	0.1856	0.512303	5		-2.9	-2.9		
VB294	45.848	191.507	0.1447	0.511638	4		-2.1	-1.6		
VB280	1.262	5.325	0.1432	0.511457	5		-5.2	-4.7		
VB280 (Repeat)	1.247	5.246	0.1436	0.511455	4		-5.4	-4.9		
VAV127	5.485	27.965	0.1185	0.511117	4	3.24		-3.7		Felsic volcanic rocks
VAV060	3.657	19.142	0.1155	0.511114	4	3.14		-2.8		
VAV003	0.251	0.974	0.1556	0.512007	3	2.99		1.3		
VAV208	2.501	12.982	0.1164	0.511336	4	2.83	2.2			

ACCEPTED MANUSCRIPT

Highlights

- Diverse types of volcanic rocks occur in the Neoarchaean Veligallu greenstone belt.
- Initially a tholeiitic basalt formed from a slightly depleted mantle in an incipient oceanic arc.
- Emplacement of mantle plume-derived komatiites and ferropicrites as the arc matured.
- Finally outpouring of various types of felsic volcanic rocks in a possible continental margin arc.
- Interplay between plume and arc was an important process of crustal evolution during Neoarchaean.

ACCEPTED MANUSCRIPT